General theoretical description of angle-resolved photoemission spectroscopy of van der Waals structures

B. Amorim*

CeFEMA, Instituto Superior Técnico, Universidade de Lisboa, Avenida Rovisco Pais, 1049-001 Lisboa, Portugal

(Received 12 November 2017; revised manuscript received 26 March 2018; published 9 April 2018)

We develop a general theory to model the angle-resolved photoemission spectroscopy (ARPES) of commensurate and incommensurate van der Waals (vdW) structures, formed by lattice mismatched and/or misaligned stacked layers of two-dimensional materials. The present theory is based on a tight-binding description of the structure and the concept of generalized umklapp processes, going beyond previous descriptions of ARPES in incommensurate vdW structures, which are based on continuous, low-energy models, being limited to structures with small lattice mismatch/misalignment. As applications of the general formalism, we study the ARPES bands and constant energy maps for two structures: twisted bilayer graphene and twisted bilayer MoS_2. The present theory should be useful in correctly interpreting experimental results of ARPES of vdW structures and other systems displaying competition between different periodicities, such as two-dimensional materials weakly coupled to a substrate and materials with density wave phases.

DOI: 10.1103/PhysRevB.97.165414

I. INTRODUCTION

The development of fabrication techniques in recent years enabled the creation of structures formed by stacked layers of different two-dimensional (2D) materials, referred to as van der Waals (vdW) structures [1–3]. By combining layers of materials displaying different properties, it is possible to engineer devices with new functionalities, not displayed by the individual layers. This makes vdW structures very appealing from the applications point of view. As examples, transistors based on graphene and hexagonal boron nitride (*h*-BN) or a semiconducting transition metal dichalcogenide (STMD) [4,5] and photodetectors based on graphene and a STMD [6–8] have already been realized. The properties of a vdW structure depend not only on the properties of the individual layers, but also on how different layers interact with each other. Due to the high crystallographic quality of 2D materials, the interlayer interaction depends crucially on the lattice mismatch and misalignment between different layers. This is clearly exemplified, both experimentally [9] and theoretically [10,11], by the observation of negative differential conductance in graphene/*h*-BN/graphene vertical tunneling transistors, where the bias voltage at which peak current occurs is controlled by the angle between the misaligned graphene electrodes. A necessary step to fully understand and take advantage of vdW structures is to characterize their electronic properties and how these depend on the lattice mismatch/misalignment.

Angle-resolved photoemission spectroscopy (ARPES) is an extensively used tool to characterize the electronic degrees of freedom of materials [12–14]. In crystals, ARPES is generally understood as a direct probe of the electronic band structure over the Brillouin zone of occupied states. Nevertheless, even in a perfect crystal where the notions of reciprocal space and Brillouin zone are well defined, this picture might break down, as the ARPES response is weighted by matrix elements which describe the light-induced electronic transition from a crystal bound state to a photoemitted electron state. For bands that are well decoupled from the remaining band structure, the ARPES matrix elements are featureless, and indeed ARPES can be seen as a direct probe of the band structure. However, exceptions to this can occur and the matrix elements can impose selection rules on the transitions. Two well known examples where this occurs are graphite [15] and graphene [16–22]. In these materials part of the Fermi surface is not observed in constant energy ARPES maps [23]. This effect is due to the ARPES matrix elements, which suppress the signal from some parts of the band structure.

Another case where the ARPES matrix elements should play an important role is in systems with competing periodicities, such as materials displaying charge density wave (CDW) phases [24,25]. In this case it is easy to understand how the interpretation of ARPES as a direct probe of the band structure can break down. Let us suppose that for a given material in the normal, undistorted phase, ARPES accurately maps the electronic band structure. Suppose that the system undergoes a transition into a commensurate CDW, with a larger unit cell. If the distortion is small, the bands in Brillouin zone will be weakly perturbed apart from backfolding into the new, smaller, Brillouin zone associated with the enlarged unit cell. If the CDW perturbation is weak, by an adiabatic argument, the ARPES mapped bands observed in both phases must be essentially unchanged. This means that the signal of the backfolded bands must be very weak, and the observed ARPES bands will mostly follow the bands of the undistorted phase, in an extended zone scheme. The suppression of the backfolded bands is encoded by the ARPES matrix elements. This was exemplified in Ref. [24] in a simple one-dimensional tight-binding model. These effects may also be relevant when

*bruno.a.c.amorim@tecnico.ulisboa.pt; amorim.bac@gmail.com

interpreting ARPES experiments in cuprates, for which a hidden density wave state has been proposed [26].

In vdW structures, such competing periodicities naturally occur due to the lattice mismatch between different layers. Therefore, a general theory capable of correctly taking into account ARPES matrix elements is essential to interpret ARPES data from vdW structures. We point out that the modeling of ARPES in twisted bilayer graphene [27] and graphene/h-BN [28] structures has been considered previously in the literature. However the models employed relied on effective low-energy, continuous descriptions of the systems, which are only valid for small misalignment angles. As the field of vdW structures develops, a more general and flexible approach is required. The goal of this work is to develop a general framework to theoretically model ARPES, which is valid for both commensurate and incommensurate structures formed by arbitrary materials and with arbitrary lattice mismatch/misalignment.

The structure of this paper is as follows. In Sec. II, we review the description of vdW structures based on tight-binding models and generalized umklapp processes developed in Refs. [29,30]. We use this description of vdW structures to compute the ARPES matrix elements for an arbitrary structure in Sec. III. We apply the general framework to model ARPES in twisted bilayer graphene and twisted bilayer MoS_2 in Sec. IV. Conclusions are drawn in Sec. V. For completeness and the convenience of the reader, in Appendix A, we briefly review the derivation of the ARPES intensity within the nonequilibrium Green's function approach [31,32]. In Appendix B, we present some details on the evaluation of the Fourier transform components of the interlayer hopping in twisted bilayer MoS_2.

II. TIGHT-BINDING DESCRIPTION OF vDW STRUCTURES

A first step in modeling ARPES of vdW structures is to describe the electronic states bound to the structure. Following Refs. [29,30], we employ a tight-binding model to describe the bound states. We will focus on bilayer structures, where each layer has a periodic structure with Bravais lattice sites given by $\{\mathbf{R}_{\ell,i}\}$, with $\ell = t,b$ labeling the top and bottom layers, respectively. The single-particle Hamiltonian of the structure is written as

$$H = H_t + H_b + H_{tb} + H_{bt}, \tag{1}$$

where H_t and H_b are the tight-binding Hamiltonians of the isolated top and bottom layers and H_{tb} (H_{bt}) describes the hopping of electrons from the bottom (top) to the top (bottom) layer. More concretely, the intralayer terms are written as

$$H_\ell = \sum_{i,j,\alpha,\beta} h^{\ell,\ell}_{\alpha\beta}(\mathbf{R}_{\ell,i},\mathbf{R}_{\ell,j}) c^\dagger_{\ell,\mathbf{R}_{\ell,i},\alpha} c_{t,\mathbf{R}_{\ell,j},\beta} \tag{2}$$

for $\ell = t,b$, and the interlayer terms as

$$H_{tb} = \sum_{i,j,\alpha,\beta} h^{t,b}_{\alpha\beta}(\mathbf{R}_{t,i},\mathbf{R}_{b,j}) c^\dagger_{t,\mathbf{R}_{t,i},\alpha} c_{b,\mathbf{R}_{b,j},\beta}, \tag{3}$$

with $H_{bt} = H^\dagger_{tb}$. In the previous equations, the indices i,j run over lattice sites and the indices α,β run over sublattice, orbital, and spin degrees of freedom. The operator $c^\dagger_{\ell,\mathbf{R}_{\ell,i},\alpha}$ creates an electron in state $|\ell,\mathbf{R}_{\ell,i},\alpha\rangle$, a localized Wannier state in layer ℓ, lattice site $\mathbf{R}_{\ell,i}$, and sublattice site $\boldsymbol{\tau}_{\ell,\alpha}$. The Wannier wave function in real space reads $\langle \mathbf{r}|\ell,\mathbf{R}_{\ell,i},\alpha\rangle = w_{\ell,\alpha}(\mathbf{r} - \mathbf{R}_{\ell,i} - \boldsymbol{\tau}_{\ell,\alpha})$ where $w_{\ell,\alpha}(\mathbf{r})$ is the Wannier wave function or type α centered on the origin. $h^{t,t}_{\alpha\beta}(\mathbf{R}_{t,i},\mathbf{R}_{t,j})$ and $h^{b,b}_{\alpha\beta}(\mathbf{R}_{b,i},\mathbf{R}_{b,j})$ are intralayer hopping terms, which we assume to be invariant under translations by lattice vector of the respective layer. $h^{t,b}_{\alpha\beta}(\mathbf{R}_{t,i},\mathbf{R}_{b,j})$ and $h^{b,t}_{\alpha\beta}(\mathbf{R}_{b,i},\mathbf{R}_{t,j})$ are interlayer hopping terms, which describe the coupling between the two layers. It is convenient to express the electronic operators in terms of Fourier components

$$c^\dagger_{\ell,\mathbf{R}_{\ell,i},\alpha} = \frac{1}{\sqrt{N_\ell}} \sum_{\mathbf{k}_\ell} e^{-i\mathbf{k}_\ell\cdot(\mathbf{R}_{\ell,i}+\boldsymbol{\tau}_{\ell,\alpha})} c^\dagger_{\ell,\mathbf{k}_\ell,\alpha}, \tag{4}$$

where $\mathbf{k}_\ell$ belongs to the Brillouin zone of layer ℓ and N_ℓ is the number of unit cells in layer ℓ. Notice that if $\mathbf{G}_\ell$ is a reciprocal lattice vector of layer ℓ, i.e., $e^{i\mathbf{G}_\ell\cdot\mathbf{R}_{\ell,i}} = 1$, then $c^\dagger_{\ell,\mathbf{k}+\mathbf{G}_\ell,\alpha} = e^{i\mathbf{G}_\ell\cdot\boldsymbol{\tau}_{\ell,\alpha}} c^\dagger_{\ell,\mathbf{k},\alpha}$. These states bring the Hamiltonians of the isolated layers to a block diagonal form,

$$H_\ell = \sum_{\mathbf{k}_\ell,\alpha,\beta} c^\dagger_{\ell,\mathbf{k}_\ell,\alpha} h^{\ell,\ell}_{\alpha\beta}(\mathbf{k}_\ell) c_{\ell,\mathbf{k}_\ell,\beta}, \tag{5}$$

where $h^{\ell,\ell}_{\alpha\beta}(\mathbf{k}_\ell) = \sum_i e^{-i\mathbf{k}_\ell\cdot(\mathbf{R}_{\ell,i}+\boldsymbol{\tau}_{\ell,\alpha}-\boldsymbol{\tau}_{\ell,\beta})} h^{\ell,\ell}_{\alpha\beta}(\mathbf{R}_{\ell,i},\mathbf{0})$. For the interlayer term, we assume a two-center approximation for the hopping elements and write them in terms of their Fourier transform components [30] as (focusing on the H_{tb} term)

$$h^{t,b}_{\alpha\beta}(\mathbf{R}_{t,i},\mathbf{R}_{b,j}) = \sqrt{A_{\mathrm{c},t} A_{\mathrm{c},b}} \times \int \frac{d^2\mathbf{q}}{(2\pi)^2} e^{i\mathbf{q}\cdot(\mathbf{R}_{t,i}+\boldsymbol{\tau}_{t,\alpha}-\mathbf{R}_{b,j}-\boldsymbol{\tau}_{b,\beta})} h^{t,b}_{\alpha\beta}(\mathbf{q}), \tag{6}$$

where $A_{\mathrm{c},\ell}$ is the area of the unit cell of layer ℓ. With this we can write H_{tb} as

$$H_{tb} = \sum_{\mathbf{k}_t,\mathbf{k}_b,\alpha,\beta} \sum_{i,j} e^{i\boldsymbol{\tau}_{t,\alpha}\cdot\mathbf{G}_{t,i}} h^{t,b}_{\alpha\beta}(\mathbf{k}_t + \mathbf{G}_{t,i}) e^{-i\boldsymbol{\tau}_{b,\beta}\cdot\mathbf{G}_{b,j}} \times c^\dagger_{t,\mathbf{k}_t+\mathbf{G}_{t,i},\alpha} c_{b,\mathbf{k}_b+\mathbf{G}_{b,j},\beta} \delta_{\mathbf{k}_t+\mathbf{G}_{t,i},\mathbf{k}_b+\mathbf{G}_{b,j}}, \tag{7}$$

where $\mathbf{G}_{\ell,i}$ are reciprocal lattice vectors of layer ℓ. H_{bt} is written in a similar way.

Equation (7) tells us that states of the two layers with crystal momentum $\mathbf{k}_t$ and $\mathbf{k}_b$ are only coupled provided $\mathbf{G}_{t,i}$ and $\mathbf{G}_{b,j}$ exist, such that the generalized umklapp condition $\mathbf{k}_t + \mathbf{G}_{t,i} = \mathbf{k}_b + \mathbf{G}_{b,j}$ is satisfied [30]. In an extended Brillouin zone scheme, the generalized umklapp condition can be satisfied if for each $\mathbf{G}_{t,i}$ and $\mathbf{G}_{b,j}$ we write $\mathbf{k}_t = \mathbf{k} + \mathbf{G}_{b,j}$ and $\mathbf{k}_b = \mathbf{k} + \mathbf{G}_{t,i}$ for any $\mathbf{k}$. This fact motivates us to look for eigenstates of the complete Hamiltonian Eq. (1) of the form

$$|\psi^{\mathrm{vdW}}_{\mathbf{k},n}\rangle = \sum_{i,\alpha} \phi^n_{t,\mathbf{k},\alpha}(\mathbf{G}_{b,i}) c^\dagger_{t,\mathbf{k}+\mathbf{G}_{b,i},\alpha}|0\rangle + \sum_{i,\alpha} \phi^n_{b,\mathbf{k},\alpha}(\mathbf{G}_{t,i}) c^\dagger_{b,\mathbf{k}+\mathbf{G}_{t,i},\alpha}|0\rangle, \tag{8}$$

with $\phi^n_{t,\mathbf{k},\alpha}(\mathbf{G}_{b,i})$ and $\phi^n_{b,\mathbf{k},\alpha}(\mathbf{G}_{t,i})$ coefficients that are to be determined. We now introduce a convenient compact notation. We define $\boldsymbol{\phi}^n_{\ell,\mathbf{k}}(\mathbf{G})$ as a vector with entries given by $[\boldsymbol{\phi}^n_{\ell,\mathbf{k}}(\mathbf{G})]_\alpha = \phi^n_{\ell,\mathbf{k},\alpha}(\mathbf{G})$. In the same way we introduce the matrices $\boldsymbol{h}^{\ell,\ell}_{\mathbf{k}}$ with entries $[\boldsymbol{h}^{\ell,\ell}_{\mathbf{k}}]_{\alpha\beta} = h^{\ell,\ell}_{\alpha\beta}(\mathbf{k})$, $\boldsymbol{h}^{t,b}_{\mathbf{k},\mathbf{G}_b,\mathbf{G}_t}$ with

entries $[\boldsymbol{h}^{t,b}_{\mathbf{k},\mathbf{G}_b,\mathbf{G}_t}]_{\alpha\beta} = e^{i\mathbf{G}_t\cdot\boldsymbol{\tau}_{t,\alpha}} h^{t,b}_{\alpha\beta}(\mathbf{k}+\mathbf{G}_b+\mathbf{G}_t) e^{-i\mathbf{G}_b\cdot\boldsymbol{\tau}_{b,\beta}}$ and $\boldsymbol{h}^{b,t}_{\mathbf{k},\mathbf{G}_t,\mathbf{G}_b}$ defined in a similar way. This allows us to write the eigenvalue problem which determines the eigenstates and energies of the vdW structure as

$$\boldsymbol{H}_{\mathbf{k}}(\{\mathbf{G}_b\},\{\mathbf{G}_t\}) \cdot \begin{bmatrix} \boldsymbol{\phi}^n_{t,\mathbf{k}}(\{\mathbf{G}_b\}) \\ \boldsymbol{\phi}^n_{b,\mathbf{k}}(\{\mathbf{G}_t\}) \end{bmatrix} = E_{\mathbf{k},n} \begin{bmatrix} \boldsymbol{\phi}^n_{t,\mathbf{k}}(\{\mathbf{G}_b\}) \\ \boldsymbol{\phi}^n_{b,\mathbf{k}}(\{\mathbf{G}_t\}) \end{bmatrix}, \quad (9)$$

where $E_{\mathbf{k},n}$ are the energies,

$$\boldsymbol{\phi}^n_{t,\mathbf{k}}(\{\mathbf{G}_b\}) = \begin{bmatrix} \boldsymbol{\phi}^n_{t,\mathbf{k}}(\mathbf{G}_{b,1}) & \boldsymbol{\phi}^n_{t,\mathbf{k}}(\mathbf{G}_{b,2}) & \cdots \end{bmatrix}^t, \quad (10)$$

$$\boldsymbol{\phi}^n_{b,\mathbf{k}}(\{\mathbf{G}_t\}) = \begin{bmatrix} \boldsymbol{\phi}^n_{b,\mathbf{k}}(\mathbf{G}_{t,1}) & \boldsymbol{\phi}^n_{b,\mathbf{k}}(\mathbf{G}_{t,2}) & \cdots \end{bmatrix}^t, \quad (11)$$

are vectors formed by the coefficients $\phi^n_{t,\mathbf{k},\alpha}(\mathbf{G}_{b,i})$ and $\phi^n_{b,\mathbf{k},\alpha}(\mathbf{G}_{t,i})$ for different $\mathbf{G}_{b,i}$ and $\mathbf{G}_{t,i}$, and the Hamiltonian matrix is written as

$$\boldsymbol{H}_{\mathbf{k}}(\{\mathbf{G}_b\},\{\mathbf{G}_t\}) = \begin{bmatrix} \boldsymbol{\mathcal{H}}^{t,t}_{\mathbf{k}+\{\mathbf{G}_b\}} & \boldsymbol{\mathcal{H}}^{t,b}_{\mathbf{k},\{\mathbf{G}_b\},\{\mathbf{G}_t\}} \\ \boldsymbol{\mathcal{H}}^{b,t}_{\mathbf{k},\{\mathbf{G}_t\},\{\mathbf{G}_b\}} & \boldsymbol{\mathcal{H}}^{b,b}_{\mathbf{k}+\{\mathbf{G}_t\}} \end{bmatrix}, \quad (12)$$

where $\boldsymbol{\mathcal{H}}^{t,t}_{\mathbf{k}+\{\mathbf{G}_b\}}$ is a block diagonal matrix

$$\boldsymbol{\mathcal{H}}^{t,t}_{\mathbf{k}+\{\mathbf{G}_b\}} = \begin{bmatrix} \boldsymbol{h}^{t,t}_{\mathbf{k}+\mathbf{G}_{b,1}} & \mathbf{0} & \cdots \\ \mathbf{0} & \boldsymbol{h}^{t,t}_{\mathbf{k}+\mathbf{G}_{b,2}} & \\ \vdots & & \ddots \end{bmatrix}, \quad (13)$$

with $\boldsymbol{\mathcal{H}}^{b,b}_{\mathbf{k}+\{\mathbf{G}_t\}}$ similarly defined, and $\boldsymbol{\mathcal{H}}^{t,b}_{\mathbf{k},\{\mathbf{G}_b\},\{\mathbf{G}_t\}}$ is a dense matrix

$$\boldsymbol{\mathcal{H}}^{t,b}_{\mathbf{k},\{\mathbf{G}_b\},\{\mathbf{G}_t\}} = \begin{bmatrix} \boldsymbol{h}^{t,b}_{\mathbf{k},\mathbf{G}_{b,1},\mathbf{G}_{t,1}} & \boldsymbol{h}^{t,b}_{\mathbf{k},\mathbf{G}_{b,1},\mathbf{G}_{t,2}} & \cdots \\ \boldsymbol{h}^{t,b}_{\mathbf{k},\mathbf{G}_{b,2},\mathbf{G}_{t,1}} & \boldsymbol{h}^{t,b}_{\mathbf{k},\mathbf{G}_{b,2},\mathbf{G}_{t,2}} & \cdots \\ \vdots & \vdots & \ddots \end{bmatrix}, \quad (14)$$

with $\boldsymbol{\mathcal{H}}^{b,t}_{\mathbf{k},\{\mathbf{G}_t\},\{\mathbf{G}_b\}} = (\boldsymbol{\mathcal{H}}^{t,b}_{\mathbf{k},\{\mathbf{G}_b\},\{\mathbf{G}_t\}})^\dagger$. For a commensurate structure, there exist $\mathbf{G}_{b,i}$ and $\mathbf{G}_{t,j}$ such that $\mathbf{G}_{b,i} = \mathbf{G}_{t,j}$ and the sums over reciprocal lattice vectors in Eq. (8) become finite, and consequently the matrix $\boldsymbol{H}_{\mathbf{k}}(\{\mathbf{G}_b\},\{\mathbf{G}_t\})$ is finite. In this case, the eigenvalues and eigenstates of $\boldsymbol{H}_{\mathbf{k}}(\{\mathbf{G}_b\},\{\mathbf{G}_t\})$ for $\mathbf{k}$ restricted to the Brillouin zone of the commensurate structure provide us the full spectrum and eigenstates of the bilayer structure. For an incommensurate structure, the sums over reciprocal lattice vectors in Eq. (8) involve an infinite number of terms and the corresponding Hamiltonian matrix $\boldsymbol{H}_{\mathbf{k}}(\{\mathbf{G}_b\},\{\mathbf{G}_t\})$ is infinite. However, an approximation to the eigenstates and energies of the incommensurate structure can still be obtained by suitably truncating $\boldsymbol{H}_{\mathbf{k}}(\{\mathbf{G}_b\},\{\mathbf{G}_t\})$, considering a finite number of reciprocal lattice vectors $\mathbf{G}_{t,i}$ and $\mathbf{G}_{b,i}$. Even in the case of a commensurate structure, the supercell might be very large, leading to a very large matrix $\boldsymbol{H}_{\mathbf{k}}(\{\mathbf{G}_b\},\{\mathbf{G}_t\})$, and in that situation it might still be beneficial to compute the eigenstates and energies of the system approximately by truncating $\boldsymbol{H}_{\mathbf{k}}(\{\mathbf{G}_b\},\{\mathbf{G}_t\})$. In the following, we will generally refer to the approximate eigenvalues $E_{\mathbf{k},n}$ as band structure, even in the case where we have an incommensurate structure and the concept of Brillouin zone no longer applies.

We will now prove a formal relation satisfied by the solutions of Eq. (9) that will be useful in the next section. Assume that

$$\begin{bmatrix} \boldsymbol{\phi}^n_{t,\mathbf{k}}(\{\mathbf{G}_b\}) \\ \boldsymbol{\phi}^n_{b,\mathbf{k}}(\{\mathbf{G}_t\}) \end{bmatrix} \quad (15)$$

is an eigenstate of $\boldsymbol{H}_{\mathbf{k}}(\{\mathbf{G}_b\},\{\mathbf{G}_t\})$ with eigenvalue $E_{\mathbf{k},n}$. Then

$$\begin{bmatrix} e^{-i\mathbf{G}_{t,j}\cdot\boldsymbol{\tau}_t} \boldsymbol{\phi}^n_{t,\mathbf{k}}(\{\mathbf{G}_b\}) \\ \boldsymbol{\phi}^n_{b,\mathbf{k}}(\{\mathbf{G}_{t,j}+\mathbf{G}_t\}) \end{bmatrix} \quad (16)$$

is an eigenstate of $\boldsymbol{H}_{\mathbf{k}+\mathbf{G}_{t,j}}(\{\mathbf{G}_b\},\{\mathbf{G}_t\})$ with the same eigenvalue. This allows us to identify

$$\phi^n_{t,\mathbf{k}+\mathbf{G}_{t,j},\alpha}(\mathbf{G}_b) = e^{-i\mathbf{G}_{t,j}\cdot\boldsymbol{\tau}_{t,\alpha}} \phi^n_{t,\mathbf{k},\alpha}(\mathbf{G}_b), \quad (17)$$

$$\phi^n_{b,\mathbf{k}+\mathbf{G}_{t,j},\alpha}(\mathbf{G}_t) = \phi^n_{b,\mathbf{k},\alpha}(\mathbf{G}_{t,j}+\mathbf{G}_t). \quad (18)$$

This statement can be proved by looking at the structure of $\boldsymbol{H}_{\mathbf{k}+\mathbf{G}_{t,j}}(\{\mathbf{G}_b\},\{\mathbf{G}_t\})$. First, we notice that

$$\left[\boldsymbol{h}^{t,t}_{\mathbf{k}+\mathbf{G}_{t,j}+\mathbf{G}_{b,i}}\right]_{\alpha\beta} = e^{-i\mathbf{G}_{t,j}\cdot\boldsymbol{\tau}_{t,\alpha}} \left[\boldsymbol{h}^{t,t}_{\mathbf{k}+\mathbf{G}_{b,i}}\right]_{\alpha\beta} e^{i\mathbf{G}_{t,j}\cdot\boldsymbol{\tau}_{t,\beta}}, \quad (19)$$

$$\left[\boldsymbol{h}^{t,b}_{\mathbf{k}+\mathbf{G}_{t,j},\mathbf{G}_b,\mathbf{G}_t}\right]_{\alpha\beta} = e^{-i\mathbf{G}_{t,j}\cdot\boldsymbol{\tau}_{t,\alpha}} \left[\boldsymbol{h}^{t,b}_{\mathbf{k},\mathbf{G}_b,\mathbf{G}_t+\mathbf{G}_{t,j}}\right]_{\alpha\beta}. \quad (20)$$

With these relations, we can write

$$\boldsymbol{H}_{\mathbf{k}+\mathbf{G}_{t,j}}(\{\mathbf{G}_b\},\{\mathbf{G}_t\}) = \begin{bmatrix} e^{-i\mathbf{G}_{t,j}\cdot\boldsymbol{\tau}_t} & \mathbf{0} \\ \mathbf{0} & \mathbf{1} \end{bmatrix} \cdot \boldsymbol{H}_{\mathbf{k}}(\{\mathbf{G}_b\},\{\mathbf{G}_t+\mathbf{G}_{t,j}\}) \cdot \begin{bmatrix} e^{i\mathbf{G}_{t,j}\cdot\boldsymbol{\tau}_t} & \mathbf{0} \\ \mathbf{0} & \mathbf{1} \end{bmatrix}. \quad (21)$$

For a commensurate structure, the set of vectors $\{\mathbf{G}_t\}$ is finite and periodic modulo reciprocal lattice vectors of the commensurate lattice. Therefore $\{\mathbf{G}_t+\mathbf{G}_{t,j}\}$ coincides with $\{\mathbf{G}_t\}$ apart from a reordering of the vectors. Assume that this reordering is implemented by a permutation matrix $\boldsymbol{P}$ such that $\boldsymbol{P}\{\mathbf{G}_t\} = \{\mathbf{G}_t+\mathbf{G}_{t,j}\}$. Since both the Hamiltonian $\boldsymbol{H}_{\mathbf{k}}(\{\mathbf{G}_b\},\{\mathbf{G}_t+\mathbf{G}_{t,j}\})$ and the vector $[\boldsymbol{\phi}^n_{t,\mathbf{k}}(\{\mathbf{G}_b\}) \quad \boldsymbol{\phi}^n_{b,\mathbf{k}}(\{\mathbf{G}_{t,j}+\mathbf{G}_t\})]^t$ are reordered in the same way, we can write

$$\boldsymbol{H}_{\mathbf{k}+\mathbf{G}_{t,j}}(\{\mathbf{G}_b\},\{\mathbf{G}_t\}) \cdot \begin{bmatrix} e^{-i\mathbf{G}_{t,j}\cdot\boldsymbol{\tau}_t} \boldsymbol{\phi}^n_{t,\mathbf{k}}(\{\mathbf{G}_b\}) \\ \boldsymbol{\phi}^n_{b,\mathbf{k}}(\{\mathbf{G}_{t,j}+\mathbf{G}_t\}) \end{bmatrix} = \begin{bmatrix} e^{-i\mathbf{G}_{t,j}\cdot\boldsymbol{\tau}_t} & \mathbf{0} \\ \mathbf{0} & \mathbf{1} \end{bmatrix} \cdot \boldsymbol{H}_{\mathbf{k}}(\{\mathbf{G}_b\},\{\mathbf{G}_t+\mathbf{G}_{t,j}\}) \cdot \begin{bmatrix} \boldsymbol{\phi}^n_{t,\mathbf{k}}(\{\mathbf{G}_b\}) \\ \boldsymbol{\phi}^n_{b,\mathbf{k}}(\{\mathbf{G}_{t,j}+\mathbf{G}_t\}) \end{bmatrix}$$

$$= \begin{bmatrix} e^{-i\mathbf{G}_{t,j}\cdot\boldsymbol{\tau}_t} & \mathbf{0} \\ \mathbf{0} & \mathbf{1} \end{bmatrix} \cdot \boldsymbol{P}\cdot\boldsymbol{P}^{-1} \cdot \boldsymbol{H}_{\mathbf{k}}(\{\mathbf{G}_b\},\{\mathbf{G}_t+\mathbf{G}_{t,j}\}) \cdot \boldsymbol{P}\cdot\boldsymbol{P}^{-1} \cdot \begin{bmatrix} \boldsymbol{\phi}^n_{t,\mathbf{k}}(\{\mathbf{G}_b\}) \\ \boldsymbol{\phi}^n_{b,\mathbf{k}}(\{\mathbf{G}_{t,j}+\mathbf{G}_t\}) \end{bmatrix}$$

$$= \begin{bmatrix} e^{-i\mathbf{G}_{t,j}\cdot\boldsymbol{\tau}_t} & \mathbf{0} \\ \mathbf{0} & \mathbf{1} \end{bmatrix} \cdot \boldsymbol{P} \cdot \boldsymbol{H}_{\mathbf{k}}(\{\mathbf{G}_b\},\{\mathbf{G}_t\}) \cdot \begin{bmatrix} \boldsymbol{\phi}^n_{t,\mathbf{k}}(\{\mathbf{G}_b\}) \\ \boldsymbol{\phi}^n_{b,\mathbf{k}}(\{\mathbf{G}_t\}) \end{bmatrix}$$

$$= E_{\mathbf{k},n}\begin{bmatrix} e^{-i\mathbf{G}_{t,j}\cdot\boldsymbol{\tau}_t} & \mathbf{0} \\ \mathbf{0} & \mathbf{1} \end{bmatrix}\cdot \boldsymbol{P}\cdot\begin{bmatrix} \boldsymbol{\phi}^n_{t,\mathbf{k}}(\{\mathbf{G}_b\}) \\ \boldsymbol{\phi}^n_{b,\mathbf{k}}(\{\mathbf{G}_t\}) \end{bmatrix} = E_{\mathbf{k},n}\begin{bmatrix} e^{-i\mathbf{G}_{t,j}\cdot\boldsymbol{\tau}_t}\boldsymbol{\phi}^n_{t,\mathbf{k}}(\{\mathbf{G}_b\}) \\ \boldsymbol{\phi}^n_{b,\mathbf{k}}(\{\mathbf{G}_{t,j}+\mathbf{G}_t\}) \end{bmatrix}, \tag{22}$$

proving our statement for the commensurate case. For an incommensurate structure, the set $\{\mathbf{G}_t\}$ is infinite and therefore, apart from a reordering, we have that $\{\mathbf{G}_{t,j}+\mathbf{G}_t\}$ and $\{\mathbf{G}_t\}$ coincide [33] and we also obtain Eq. (22). This proves our formal statement for both the commensurate and the incommensurate cases. Following the same argumentation it can also be formally shown that

$$\phi^n_{t,\mathbf{k}+\mathbf{G}_{b,j},\alpha}(\mathbf{G}_b) = \phi^n_{t,\mathbf{k},\alpha}(\mathbf{G}_b+\mathbf{G}_{b,j}), \tag{23}$$

$$\phi^n_{b,\mathbf{k}+\mathbf{G}_{b,j},\alpha}(\mathbf{G}_t) = e^{-i\mathbf{G}_{b,j}\cdot\boldsymbol{\tau}_{t,\alpha}}\phi^n_{b,\mathbf{k},\alpha}(\mathbf{G}_t). \tag{24}$$

In this section, the coupling between the two layers was assumed to only give origin to interlayer hopping terms, not affecting the intralayer Hamiltonians H_t and H_b, which were assumed to preserve the translational symmetry of the isolated layers. Besides this effect, there is also the possibility of one of the layers inducing a potential to which the electrons in the other layer will be subjected [34–36]. The coupling between the layers can also lead to structural relaxation, which gives origin to a modulation of the intralayer hoppings due to the displacement of the atomic positions [37–40]. Although we will not explore those effects in the present work, we note that these corrections will have a spatial modulation given by $\mathbf{G}_{t,i}-\mathbf{G}_{b,j}$ and can therefore be incorporated in the present formalism by including off-diagonal blocks in the matrices $\boldsymbol{\mathcal{H}}^{t,t}_{\mathbf{k}+\{\mathbf{G}_b\}}$ and $\boldsymbol{\mathcal{H}}^{b,b}_{\mathbf{k}+\{\mathbf{G}_b\}}$ of the form

$$\left[\boldsymbol{V}^{t,t(b,b)}_{\mathbf{k}+\mathbf{G}_{b(t),i},\mathbf{k}+\mathbf{G}_{b(t),j}}\right]_{\alpha\beta} = \langle t(b),\mathbf{k}+\mathbf{G}_{b(t),i},\alpha|V^{t(b)}|t(b),\mathbf{k}+\mathbf{G}_{b(t),j},\beta\rangle, \tag{25}$$

where $V^{t(b)}$ describes the potential or intralayer hopping modulation on the top (bottom) layer and $|\ell,\mathbf{k},\alpha\rangle$ is the state created by the operator $c^\dagger_{\ell,\mathbf{k},\alpha}$ in Eq. (4).

III. ARPES IN vDW STRUCTURES

We wish to model an experimental situation where the incident electromagnetic field is monochromatic with frequency $\omega_0>0$, and the electron detector is placed at position $\mathbf{r}$, far away from the crystal sample, collecting electrons emitted with energy E along the direction $\hat{\mathbf{r}}$. In this situation, the energy-resolved ARPES intensity can be evaluated from [31,32,41–45] (see also Appendix A for a brief derivation)

$$I_{\mathrm{ARPES}}(E,\hat{\mathbf{r}}) \propto \sum_a f(E-\omega_0-\mu) \times |M_{E,\hat{\mathbf{r}};a}(\omega_0)|^2\frac{1}{2\pi}\mathcal{A}_a(E-\omega_0), \tag{26}$$

where μ is the chemical potential, the index a runs over crystal bound states, with corresponding wave function $\psi_a(\mathbf{r})$; $\mathcal{A}_a(E)$ is the spectral function, which in the noninteracting limit reduces to $\mathcal{A}_a(E)=2\pi\delta(E-\epsilon_\alpha)$, where ϵ_a is the energy of state a, and $M_{E,\hat{\mathbf{r}};a}(\omega_0)$ are the ARPES matrix elements. These are given by

$$M_{E,\hat{\mathbf{r}};a}(\omega_0) = -i\frac{e}{\hbar}\int d^3\mathbf{r}_1\{\psi^*_{E,\hat{\mathbf{r}}}(\mathbf{r}_1)[\nabla\psi_a(\mathbf{r}_1)] - [\nabla\psi^*_{E,\hat{\mathbf{r}}}(\mathbf{r}_1)]\psi_a(\mathbf{r}_1)\}\cdot\mathbf{A}_{\omega_0}(\mathbf{r}_1), \tag{27}$$

where $\mathbf{A}_{\omega_0}(\mathbf{r}_1)$ is the screened [32] vector potential and $\psi^*_{E,\hat{\mathbf{r}}}(\mathbf{r}_1)$ is the complex conjugate of a photoemitted state with energy E, which is the solution of the Lippmann-Schwinger equation

$$\psi^*_{E,\hat{\mathbf{r}}}(\mathbf{r}_1) = e^{-i\mathbf{p}_E\cdot\mathbf{r}_1} + \int d^3\mathbf{r}'\psi^*_{E,\hat{\mathbf{r}}}(\mathbf{r}')V(\mathbf{r}')G^R_{\mathrm{free}}(E;\mathbf{r}',\mathbf{r}_1), \tag{28}$$

where $\mathbf{p}_E=p_E\hat{\mathbf{r}}$, with $p_E=\sqrt{2m(E+i0^+)/\hbar^2}$, $G^R_{\mathrm{free}}(E;\mathbf{r},\mathbf{r}')$ is the free space electronic Green's function [which is explicitly given by Eq. (A19)], and $V(\mathbf{r})$ is the crystal potential. Using integration by parts, we can write the ARPES matrix element as

$$M_{E,\hat{\mathbf{r}};a}(\omega_0) = i\frac{2e}{\hbar}\int d^3\mathbf{r}_1[\nabla\psi^*_{E,\hat{\mathbf{r}}}(\mathbf{r}_1)]\psi_a(\mathbf{r}_1)\cdot\mathbf{A}_{\omega_0}(\mathbf{r}_1), \tag{29}$$

where we have neglected the contribution arising from $\nabla\cdot\mathbf{A}_{\omega_0}(\mathbf{r})=\rho/(i\omega\epsilon_0)$, where ρ is the total charge in the crystal, which is a common approximation [32,45,46]. In the same spirit, we neglect effects of screening in $\mathbf{A}_{\omega_0}(\mathbf{r}_1)$ and assume it to be described by a plane wave $\mathbf{A}_{\omega_0}(\mathbf{r}_1)=A^\lambda_{\omega_0}\mathbf{e}^\lambda_{\mathbf{q}}e^{i\mathbf{q}\cdot\mathbf{r}_1}$, where $A^\lambda_{\omega_0}$ is the amplitude, $\mathbf{q}$ is the wave vector, satisfying $\omega_0=c|\mathbf{q}|$ with c the speed of light, and $\mathbf{e}^\lambda_{\mathbf{q}}$ is the polarization vector for the $\lambda=s,p$ polarizations. For simplicity we will also approximate $\psi^*_{E,\hat{\mathbf{r}}}(\mathbf{r}_1)$ by a plane wave $\psi^*_{E,\hat{\mathbf{r}}}(\mathbf{r}_1)\simeq e^{-i\mathbf{p}_E\cdot\mathbf{r}_1}$ [15], which will greatly simplify the evaluation of $M_{E,\hat{\mathbf{r}};a}(\omega_0)$, while providing a nontrivial description of the ARPES matrix elements [47]. With these approximations we obtain

$$M_{E,\hat{\mathbf{r}};a}(\omega_0) \simeq \frac{2e}{\hbar}A^\lambda_{\omega_0}(\mathbf{p}_E\cdot\mathbf{e}^\lambda_{\mathbf{q}})\int d^3\mathbf{r}_1 e^{-i(\mathbf{p}_E-\mathbf{q})\cdot\mathbf{r}_1}\psi_a(\mathbf{r}_1) \tag{30}$$

and the ARPES matrix element becomes proportional to the Fourier transform of the crystal bound state.

In order to obtain the ARPES intensity for a bilayer vdW structure we need to evaluate Eq. (30) with the crystal bound state given by Eq. (8). In real space we have that

$$\begin{aligned}\psi^{\mathrm{vdW}}_{\mathbf{k},n}(\mathbf{r}) = {}& \frac{1}{\sqrt{N_t}}\sum_{i,j,\alpha}\phi^n_{t,\mathbf{k},\alpha}(\mathbf{G}_{b,i})e^{i(\mathbf{k}+\mathbf{G}_{b,i})\cdot(\mathbf{R}_{t,j}+\boldsymbol{\tau}_{t,\alpha})} \\ & \times w_{t,\alpha}(\mathbf{r}-\mathbf{R}_{t,j}-\boldsymbol{\tau}_{t,\alpha}) \\ & + \frac{1}{\sqrt{N_b}}\sum_{i,j,\alpha}\phi^n_{b,\mathbf{k},\alpha}(\mathbf{G}_{t,i})e^{i(\mathbf{k}+\mathbf{G}_{t,i})\cdot(\mathbf{R}_{b,j}+\boldsymbol{\tau}_{b,\alpha})} \\ & \times w_{b,\alpha}(\mathbf{r}-\mathbf{R}_{b,j}-\boldsymbol{\tau}_{b,\alpha}),\end{aligned} \tag{31}$$

and the ARPES matrix element Eq. (30) becomes

$$M_{E,\hat{\mathbf{r}};\mathbf{k},n}(\omega_0) = \frac{2e}{\hbar} A^{\lambda}_{\omega_0}\left(\mathbf{p}_E \cdot \mathbf{e}^{\lambda}_{\mathbf{q}}\right)\sqrt{N_t} \times \Bigg[\sum_{i,j,\alpha} \phi^n_{t,\mathbf{k},\alpha}(\mathbf{G}_{b,i}) e^{i\mathbf{G}_{t,j}\cdot\boldsymbol{\tau}_{t,\alpha}} e^{-iQ_z\tau^z_{t,\alpha}} \tilde{w}_{t,\alpha}(\mathbf{Q}) \delta_{\mathbf{k}+\mathbf{G}_{b,i}-\mathbf{Q}_\perp,\mathbf{G}_{t,j}} + \sqrt{\frac{N_b}{N_t}} \sum_{i,j,\alpha} \phi^n_{b,\mathbf{k},\alpha}(\mathbf{G}_{t,i}) e^{i\mathbf{G}_{b,j}\cdot\boldsymbol{\tau}_{b,\alpha}} e^{-iQ_z\tau^z_{b,\alpha}} \times \tilde{w}_{b,\alpha}(\mathbf{Q}) \delta_{\mathbf{k}+\mathbf{G}_{t,i}-\mathbf{Q}_\perp,\mathbf{G}_{b,j}} \Bigg], \tag{32}$$

where $\mathbf{Q} = \mathbf{p}_E - \mathbf{q}$ is the transferred momentum, with Q_z and $\mathbf{Q}_\perp$ indicating the components parallel and perpendicular to the z axis, and $\tilde{w}_{\ell,\alpha}(\mathbf{Q}) = \int d^3\mathbf{r} e^{-i\mathbf{Q}\cdot\mathbf{r}} w_{\ell,\alpha}(\mathbf{r})$ is the Fourier transform of the Wannier wave functions. Using the relations given by Eqs. (17), (18), (23), and (24) together with the in-plane momentum-conserving Kronecker symbols, we can write

$$\phi^n_{t,\mathbf{k},\alpha}(\mathbf{G}_{b,i}) e^{i\mathbf{G}_{t,j}\cdot\boldsymbol{\tau}_{t,\alpha}} = \phi^n_{t,\mathbf{Q}_\perp+\mathbf{G}_{t,j}-\mathbf{G}_{b,i},\alpha}(\mathbf{G}_{b,i}) e^{i\mathbf{G}_{t,j}\cdot\boldsymbol{\tau}_{t,\alpha}} = \phi^n_{t,\mathbf{Q}_\perp,\alpha}(\mathbf{0}), \tag{33}$$

$$\phi^n_{b,\mathbf{k},\alpha}(\mathbf{G}_{t,i}) e^{i\mathbf{G}_{b,j}\cdot\boldsymbol{\tau}_{b,\alpha}} = \phi^n_{b,\mathbf{Q}_\perp+\mathbf{G}_{b,j}-\mathbf{G}_{t,i},\alpha}(\mathbf{G}_{t,i}) e^{i\mathbf{G}_{b,j}\cdot\boldsymbol{\tau}_{b,\alpha}} = \phi^n_{b,\mathbf{Q}_\perp,\alpha}(\mathbf{0}), \tag{34}$$

and the ARPES matrix elements can be rewritten as

$$M_{E,\hat{\mathbf{r}};\mathbf{k},n}(\omega_0) = \sqrt{N_t}\frac{2e}{\hbar} A^{\lambda}_{\omega_0}\left(\mathbf{p}_E \cdot \mathbf{e}^{\lambda}_{\mathbf{q}}\right)\mathcal{M}_{\mathbf{Q},n} \times \sum_{i,j} \delta_{\mathbf{k}-\mathbf{Q}_\perp,\mathbf{G}_{b,i}+\mathbf{G}_{t,j}}, \tag{35}$$

where we have defined

$$\mathcal{M}_{\mathbf{Q},n} = \sum_\alpha \phi^n_{t,\mathbf{Q}_\perp,\alpha}(\mathbf{0}) e^{-iQ_z\tau^z_{t,\alpha}} \tilde{w}_{t,\alpha}(\mathbf{Q}) + \sqrt{\frac{A_{c,t}}{A_{c,b}}} \sum_\alpha \phi^n_{b,\mathbf{Q}_\perp,\alpha}(\mathbf{0}) e^{-iQ_z\tau^z_{b,\alpha}} \tilde{w}_{b,\alpha}(\mathbf{Q}), \tag{36}$$

and assumed that the total area of both layers is the same, that is $N_t A_{c,t} = N_b A_{c,b}$ [30]. It is still necessary to evaluate $\tilde{w}_{\ell,\alpha}(\mathbf{Q})$. Assuming that the Wannier functions are well localized they can be written in a separable form as [15]

$$w_{\ell,\alpha}(\mathbf{r}) = R_{\ell,\alpha}(|\mathbf{r}|)\mathcal{Y}^{m_\alpha}_{l_\alpha}(\hat{\mathbf{r}}), \tag{37}$$

where $R_{\ell,\alpha}(|\mathbf{r}|)$ is the radial wave function and $\mathcal{Y}^m_l(\hat{\mathbf{r}}) = N^m_l(-1)^{|m|}P^{|m|}_l(\cos\theta_{\hat{\mathbf{r}}})\Phi_m(\phi_{\hat{\mathbf{r}}})$ are real spherical harmonics, where

$$N^m_l = \sqrt{\frac{(2l+1)}{2\pi}\frac{(l-|m|)!}{(l+|m|)!}} \tag{38}$$

is a normalization factor, $P^m_l(x)$ is an associated Legendre polynomial, and $\Phi_m(\phi_{\hat{\mathbf{r}}})$ is defined as

$$\Phi_m(\phi_{\hat{\mathbf{r}}}) = \begin{cases} \cos(m\phi_{\hat{\mathbf{r}}}), & m > 0, \\ \frac{1}{\sqrt{2}}, & m = 0, \\ \sin(|m|\phi_{\hat{\mathbf{r}}}), & m < 0. \end{cases} \tag{39}$$

Using the plane wave expansion [48]

$$e^{-i\mathbf{Q}\cdot\mathbf{r}} = 4\pi \sum_{l=0}^{+\infty}\sum_{m=-l}^{l} (-i)^l j_l(Qr)\mathcal{Y}^m_l(\hat{\mathbf{Q}})\mathcal{Y}^m_l(\hat{\mathbf{r}}), \tag{40}$$

where $j_l(x)$ is a spherical Bessel function, we can write $\tilde{w}_{\ell,\alpha}(\mathbf{Q})$ as

$$\tilde{w}_{\ell,\alpha}(\mathbf{Q}) = (-i)^{l_\alpha}\mathcal{Y}^{m_\alpha}_{l_\alpha}(\hat{\mathbf{Q}})\tilde{R}_{\ell,\alpha}(Q), \tag{41}$$

where $\tilde{R}_{\ell,\alpha}(Q) = 4\pi\int_0^{+\infty} dr r^2 j_{l_\alpha}(Qr)R_{\ell,\alpha}(r)$ and we have used the orthogonality property of the real spherical harmonics. For the case in which $R_{\ell,\alpha}(r)$ are given by hydrogen-like wave functions

$$R_{\ell,\alpha}(r) = \frac{2}{n_\alpha a_*^{3/2}}\mathcal{N}_{n_\alpha,l_\alpha} e^{-\frac{1}{2}u} x^{l_\alpha} L^{l_\alpha+1}_{n_\alpha-l_\alpha-1}(x), \tag{42}$$

where $\mathcal{N}_{n,l} = \sqrt{(n-l-1)!/(n+l)!}$, $x = 2r/(n_\alpha a_*)$, $a_* = a_0/Z_*$ (with a_0 the Bohr radius and Z_* the effective nuclear charge), and L^α_n is a generalized Laguerre polynomial, then $\tilde{R}_{\ell,\alpha}(Q)$ can be evaluated analytically and is given by [14,49]

$$\tilde{R}_{\ell,\alpha}(Q) = 4\pi a_*^{3/2}\mathcal{N}_{n_\alpha,l_\alpha} n_\alpha^2 2^{2l_\alpha+2} l_\alpha! \times \frac{y^{l_\alpha}}{(y^2+1)^{l_\alpha+2}} C^{l_\alpha+1}_{n_\alpha-l_\alpha-1}\left(\frac{y^2-1}{y^2+1}\right), \tag{43}$$

where $y = n_\alpha Q/a_*$ and C^α_n is a Gegenbauer polynomial. Analytic expressions for $\tilde{R}_{\ell,\alpha}(Q)$ are also available if $R_{\ell,\alpha}(r)$ are approximated by Slater type [50] or Gaussian type [51] orbitals.

Summarizing the results of this section, we can write the ARPES intensity corresponding to photoemitted electrons with energy $E > 0$ emitted along direction $\hat{\mathbf{r}}$, due to an incident electromagnetic field with frequency ω_0, wave number $\mathbf{q}$, and polarization vector $\mathbf{e}^\lambda_{\mathbf{q}}$ as

$$I_{\mathrm{ARPES}}(E,\hat{\mathbf{r}} \mid \omega_0,\mathbf{q},\lambda) \propto N_t \left|\frac{2e}{\hbar}A^\lambda_{\omega_0}\right|^2 \left|\mathbf{p}_E \cdot \mathbf{e}^\lambda_{\mathbf{q}}\right|^2 \times \sum_n f(E-\omega_0-\mu)|\mathcal{M}_{\mathbf{Q},n}|^2 \frac{1}{2\pi}\mathcal{A}_{\mathbf{Q}_\perp,n}(E-\omega_0), \tag{44}$$

where $\mathbf{p}_E = p_E\hat{\mathbf{r}}$ with $p_E = \sqrt{2mE/\hbar^2}$, $\mathbf{Q} = \mathbf{p}_E - \mathbf{q}$,

$$\mathcal{M}_{\mathbf{Q},n} = \sum_\alpha \phi^n_{t,\mathbf{Q}_\perp,\alpha}(\mathbf{0}) e^{-iQ_z\tau^z_{t,\alpha}}(-i)^{l_\alpha}\mathcal{Y}^{m_\alpha}_{l_\alpha}(\hat{\mathbf{Q}})\tilde{R}_{t,\alpha}(Q) + \sqrt{\frac{A_{c,t}}{A_{c,b}}}\sum_\alpha \phi^n_{b,\mathbf{Q}_\perp,\alpha}(\mathbf{0}) e^{-iQ_z\tau^z_{b,\alpha}} \times (-i)^{l_\alpha}\mathcal{Y}^{m_\alpha}_{l_\alpha}(\hat{\mathbf{Q}})\tilde{R}_{b,\alpha}(Q), \tag{45}$$

and in order to include broadening effects we can approximate the spectral function by a Lorentzian

$$\mathcal{A}_{\mathbf{Q}_\perp,n}(\omega) \simeq 2\frac{\eta}{(\omega - E_{\mathbf{Q}_\perp,n})^2+\eta^2}, \tag{46}$$

with η the broadening factor.

We make two remarks regarding Eq. (45). First, we point out that its form depends on the chosen convention to define the Fourier components of the electronic operators in Eq. (4). It is also possible to work with an alternative convention, where

$$c^{\dagger}_{\ell,\mathbf{R}_{\ell,i},\alpha} = \frac{1}{\sqrt{N_\ell}} \sum_{\mathbf{k}_\ell} e^{-i\mathbf{k}_\ell\cdot\mathbf{R}_{\ell,i}} \tilde{c}^{\dagger}_{\ell,\mathbf{k}_\ell,\alpha}. \tag{47}$$

The operators $c^{\dagger}_{\ell,\mathbf{k}_\ell,\alpha}$ and $\tilde{c}^{\dagger}_{\ell,\mathbf{k}_\ell,\alpha}$ are related via $\tilde{c}^{\dagger}_{\ell,\mathbf{k}_\ell,\alpha} = e^{-i\mathbf{k}_\ell\cdot\boldsymbol{\tau}_{\ell,\alpha}} c^{\dagger}_{\ell,\mathbf{k}_\ell,\alpha}$. Using the convention of Eq. (47), Eq. (31) would be written as

$$\begin{aligned}\psi^{\mathrm{vdW}}_{\mathbf{k},n}(\mathbf{r}) = {} & \frac{1}{\sqrt{N_t}} \sum_{i,j,\alpha} \tilde{\phi}^{n}_{t,\mathbf{k},\alpha}(\mathbf{G}_{b,i}) e^{i(\mathbf{k}+\mathbf{G}_{b,i})\cdot\mathbf{R}_{t,j}} \\ & \times w_{t,\alpha}(\mathbf{r}-\mathbf{R}_{t,j}-\boldsymbol{\tau}_{t,\alpha}) \\ & + \frac{1}{\sqrt{N_b}} \sum_{i,j,\alpha} \tilde{\phi}^{n}_{b,\mathbf{k},\alpha}(\mathbf{G}_{t,i}) e^{i(\mathbf{k}+\mathbf{G}_{t,i})\cdot\mathbf{R}_{b,j}} \\ & \times w_{b,\alpha}(\mathbf{r}-\mathbf{R}_{b,j}-\boldsymbol{\tau}_{b,\alpha}),\end{aligned} \tag{48}$$

where $\tilde{\phi}^{n}_{t,\mathbf{k},\alpha}(\mathbf{G}_{b,i}) = \phi^{n}_{t,\mathbf{k},\alpha}(\mathbf{G}_{b,i}) e^{i(\mathbf{k}+\mathbf{G}_{b,i})\cdot\boldsymbol{\tau}_{t,\alpha}}$ and $\tilde{\phi}^{n}_{b,\mathbf{k},\alpha}(\mathbf{G}_{t,i}) = \phi^{n}_{b,\mathbf{k},\alpha}(\mathbf{G}_{t,i}) e^{i(\mathbf{k}+\mathbf{G}_{t,i})\cdot\boldsymbol{\tau}_{b,\alpha}}$. With these definitions, $\mathcal{M}_{\mathbf{Q},n}$ would be obtained from Eq. (45) by replacing $\phi^{n}_{\ell,\mathbf{Q}_\perp,\alpha}(\mathbf{0}) \to \tilde{\phi}^{n}_{\ell,\mathbf{Q}_\perp,\alpha}(\mathbf{0}) e^{-i\mathbf{Q}_\perp\cdot\boldsymbol{\tau}_{\ell,\alpha}}$. Second, we would like to emphasize that the factors of $\Phi_{m_\alpha}(\phi_{\hat{\mathbf{Q}}})$, which are included in Eq. (45) via $\mathcal{Y}^{m_\alpha}_{l_\alpha}(\hat{\mathbf{Q}})$, ensure that the ARPES intensity has the same symmetries under rotations along the z direction as the bilayer vdW structure.

We would like to point out that the present formalism can also be applied to model ARPES in other system subject to competing periodicities, such as systems displaying CDWs [52] or 2D materials weakly coupled to a substrate.

IV. APPLICATIONS

We will now apply the general formalism developed in the previous section to two systems: twisted bilayer graphene and twisted bilayer MoS_2.

A. ARPES of twisted bilayer graphene

Graphene has a triangular Bravais lattice, with a unit cell containing two carbon atoms, A and B, which form a honeycomb structure. We write the basis vectors for the bottom layer as

$$\mathbf{a}_{b,1} = a\left(\frac{1}{2},\frac{\sqrt{3}}{2}\right), \tag{49}$$

$$\mathbf{a}_{b,2} = a\left(-\frac{1}{2},\frac{\sqrt{3}}{2}\right), \tag{50}$$

where $a \simeq 2.46$Å is the graphene lattice parameter, and the positions of the A and B atoms are given by the sublattice vectors

$$\boldsymbol{\tau}_{b,A} = (0,0), \tag{51}$$

$$\boldsymbol{\tau}_{b,B} = \frac{a}{\sqrt{3}}(0,1). \tag{52}$$

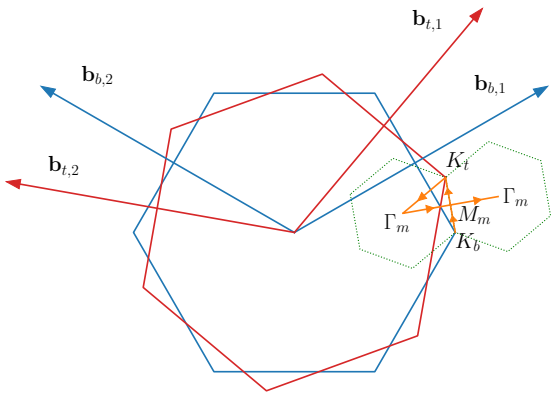

FIG. 1. Brillouin zone and basis vectors of reciprocal lattice for the top (in red) and bottom (in blue) isolated graphene layers that form a twisted bilayer graphene vdW structure. The dashed green hexagon shows the Brillouin zone of the moiré superlattice. The yellow arrows show the path along which the ARPES mapped band structure of Fig. 3 is computed.

The top layer is rotated with respect to the bottom one by an angle of θ such that $\mathbf{a}_{t,i} = R(\theta)\cdot\mathbf{a}_{b,i}$, for $i = 1,2$, and $\boldsymbol{\tau}_{t,\alpha} = R(\theta)\cdot\boldsymbol{\tau}_{b,\alpha} + d\mathbf{e}_z$, for $\alpha = A,B$, where $R(\theta)$ is the rotation matrix

$$R(\theta) = \begin{bmatrix}\cos\theta & -\sin\theta \\ \sin\theta & \cos\theta\end{bmatrix}, \tag{53}$$

and $d \simeq 3.35$Å is the separation between the two layers. The corresponding reciprocal space basis vectors are given by

$$\mathbf{b}_{b,1} = \frac{4\pi}{\sqrt{3}a}\left(\frac{\sqrt{3}}{2},\frac{1}{2}\right), \tag{54}$$

$$\mathbf{b}_{b,2} = \frac{4\pi}{\sqrt{3}a}\left(-\frac{\sqrt{3}}{2},\frac{1}{2}\right), \tag{55}$$

for the bottom layer, and by $\mathbf{b}_{t,i} = R(\theta)\cdot\mathbf{b}_{b,i}$ for the top layer. In Fig. 1, we show the first Brillouin zone of both layers. Also shown is the Brillouin zone of the moiré superlattice, whose associated reciprocal lattice basis vectors are given by $\mathbf{b}_{m,i} = \mathbf{b}_{t,i} - \mathbf{b}_{b,i}$ [53,54].

We will describe each individual graphene layer within the nearest-neighbor tight-binding model for p_z orbitals [55], which reads

$$H_\ell = -t\sum_i \sum_{j=0}^{2} (c^{\dagger}_{\ell,\mathbf{R}_{\ell,i},A} c_{\ell,\mathbf{R}_{\ell,i}+\mathbf{a}_{\ell,j},B} + \mathrm{H.c.}), \tag{56}$$

where $t \simeq 2.7$ eV is the nearest-neighbor hopping and we have written $\mathbf{a}_{\ell,0} = (0,0)$. For the interlayer coupling, we have $h^{t,b}_{\alpha\beta}(\mathbf{R}_{t,i},\mathbf{R}_{b,j}) = h^{tb}(\mathbf{R}_{t,i}+\boldsymbol{\tau}_{t,\alpha}-\mathbf{R}_{b,j}-\boldsymbol{\tau}_{b,\beta})$, $\alpha,\beta = A,B$, where the function $h^{tb}(\mathbf{r})$ can be written in terms of Slater-Koster parameters [56] as

$$h^{tb}(\mathbf{r}) = h^{tb}(\mathbf{r},d) = V_{pp\pi}(R)\frac{r^2}{R^2} + V_{pp\sigma}(R)\frac{d^2}{R^2}, \tag{57}$$

where $R = \sqrt{r^2+d^2}$ is the distance between the two atoms, with r the distance projected in the x-y plane. For the dependence of the Slater-Koster parameters on R,

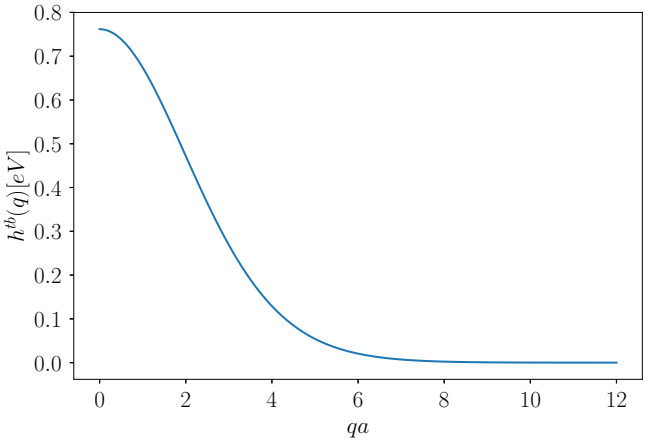

FIG. 2. Plot of the interlayer coupling function $h^{tb}(\mathbf{q})$ for bilayer graphene, Eq. (58), as a function of qa, with a the lattice parameter of graphene. The parameters used are given in the main text.

we use the parametrization of Refs. [30,57]: $V_{pp\pi}(R) = V^0_{pp\pi} e^{-(R-a/\sqrt{3})/r_0}$ and $V_{pp\sigma}(R) = V^0_{pp\sigma} e^{-(R-d)/r_0}$, where $r_0 \simeq 0.184a$, $V^0_{pp\pi} = -t \simeq -2.7$ eV, and $V^0_{pp\sigma} \simeq 0.48$ eV. From this we can evaluate numerically

$$h^{tb}_{\alpha\beta}(\mathbf{q}) = h^{tb}(\mathbf{q}) = \frac{1}{A_c}\int d^2\mathbf{r} e^{-i\mathbf{q}\cdot\mathbf{r}} h^{tb}(\mathbf{r},d), \qquad (58)$$

where $A_c = A_{c,\ell} = \sqrt{3}a^2/2$. We plot the function $h^{tb}(\mathbf{q})$ in Fig. 2.

Writing the electronic creation and annihilation operators in terms of Fourier components as in Eq. (4), we can construct the Hamiltonian for the graphene bilayer structure in the form of Eqs. (12)–(14), where

$$\boldsymbol{h}^{\ell,\ell}_{\mathbf{k}} = \begin{bmatrix} 0 & \gamma_{\ell,\mathbf{k}} \\ \gamma^*_{\ell,\mathbf{k}} & 0 \end{bmatrix} \qquad (59)$$

is written in the A,B sublattice basis, $\gamma_{\ell,\mathbf{k}} = -t\sum_{i=1}^{3} e^{i\mathbf{k}\cdot\boldsymbol{\delta}_{\ell,i}}$, with $\boldsymbol{\delta}_{\ell,i} = R(2\pi(i-1)/3)\cdot\boldsymbol{\tau}_{\ell,B}$ the nearest-neighbor vectors in each layer, and the interlayer coupling matrices are given by

$$\boldsymbol{h}^{t,b}_{\mathbf{k},\mathbf{G}_b,\mathbf{G}_t} = \begin{bmatrix} e^{i\mathbf{G}_t\cdot\boldsymbol{\tau}_{t,A}} & 0 \\ 0 & e^{i\mathbf{G}_t\cdot\boldsymbol{\tau}_{t,B}} \end{bmatrix} \cdot \begin{bmatrix} h^{tb}(\mathbf{k}+\mathbf{G}_b+\mathbf{G}_t) & h^{tb}(\mathbf{k}+\mathbf{G}_b+\mathbf{G}_t) \\ h^{tb}(\mathbf{k}+\mathbf{G}_b+\mathbf{G}_t) & h^{tb}(\mathbf{k}+\mathbf{G}_b+\mathbf{G}_t) \end{bmatrix} \cdot \begin{bmatrix} e^{-i\mathbf{G}_b\cdot\boldsymbol{\tau}_{b,A}} & 0 \\ 0 & e^{-i\mathbf{G}_b\cdot\boldsymbol{\tau}_{b,B}} \end{bmatrix}, \qquad (60)$$

with $\boldsymbol{h}^{b,t}_{\mathbf{k},\mathbf{G}_t,\mathbf{G}_b} = \left(\boldsymbol{h}^{t,b}_{\mathbf{k},\mathbf{G}_b,\mathbf{G}_t}\right)^\dagger$. By truncating the Hamiltonian to the N_G shortest $\mathbf{G}_t$ and $\mathbf{G}_b$ vectors, $\boldsymbol{H}_{\mathbf{k}}(\{\mathbf{G}_b\},\{\mathbf{G}_t\})$ becomes a $4N_G \times 4N_G$ matrix, from which we can obtain an approximation to the energies and eigenstates of the twisted bilayer graphene structure. The obtained model is a tight-binding extension of the continuous models of Refs. [57–60]. From the eigenstates, we can obtain the ARPES intensity using Eqs. (44) and (45). Due to the fact that the function $h^{tb}(\mathbf{q})$ decays rapidly for $|\mathbf{q}|a \gg 1$, the obtained ARPES signal converges rapidly with only a few $\mathbf{G}_t$ and $\mathbf{G}_b$ vectors. Notice that due to the fact that the model we use only involves $p_z \equiv \mathcal{Y}^0_1$ orbitals, we have that $\Phi_0(\phi_{\hat{\mathbf{Q}}}) = 1/\sqrt{2}$ in Eq. (45) for $\mathcal{M}_{\mathbf{Q},n}$.

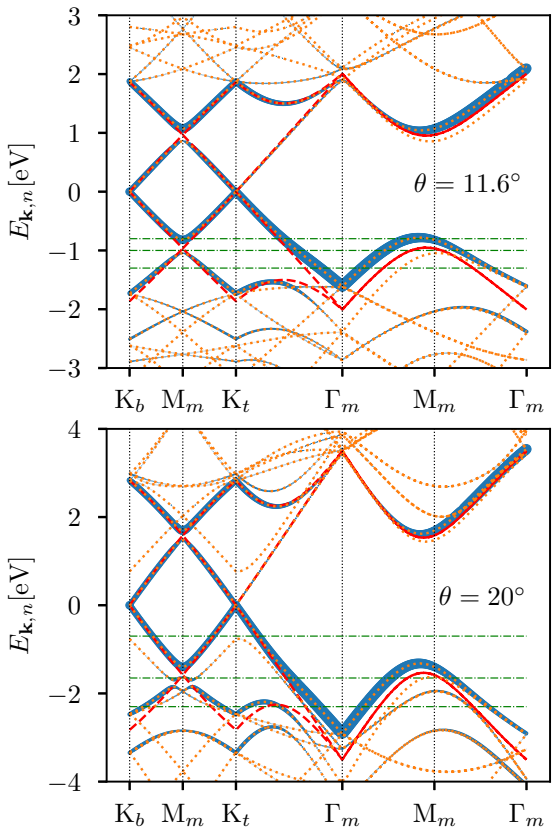

FIG. 3. Computed ARPES bands for twisted bilayer graphene for two different twist angles: $\theta = 11.6°$ (top) and $\theta = 20°$ (bottom). The yellow dotted lines show the bands $E_{\mathbf{k},n}$, eigenvalues of $\boldsymbol{H}_{\mathbf{k}}(\{\mathbf{G}_b\},\{\mathbf{G}_t\})$, for $\mathbf{k}$ along the path $K_b \to M_m \to K_t \to \Gamma_m \to M_m \to \Gamma_m$ represented by the yellow arrows in Fig. 1. The blue tick bands represent $E_{\mathbf{k},n}$ weighted by the ARPES matrix element value, with the thickness corresponding to $|\mathcal{M}_{\mathbf{k},0,n}|^2$. The dashed red lines show the dispersion relation for the decoupled graphene layers. It was assumed $Q_z = 0$. The horizontal dot-dashed lines mark the energies -1.3, -1.0, and -0.8 eV (for $\theta = 11.6°$) and -2.3, -1.65, and -0.7 eV (for $\theta = 20°$) at which the ARPES constant energy maps of Fig. 4 are computed. In both plots we used a number of reciprocal lattice vectors $N_G = 7$. It was assumed $Q_z = 0$.

In Fig. 3 we show the computed ARPES bands along the path indicated in Fig. 1, for two different angles: $\theta = 11.6°$, for which ARPES measurements where performed in Ref. [61], and for $\theta = 20°$. The thickness of the bands is proportional to the value of $|\mathcal{M}_{\mathbf{Q}_\perp,0,n}|^2$, where for simplicity we assumed that there is no transferred momentum along the z direction, $Q_z = 0$, and neglected the effect of $\tilde{R}_{\ell,\alpha}(Q)$ on $\mathcal{M}_{\mathbf{Q}_\perp,0,n}$. The bands where computed using a truncated Hamiltonian with $N_G = 7$ [including $\mathbf{G}_{b/t} = (0,0)$], which was found to be sufficient to obtain converged results. Increasing N_G virtually does not change the thick bands in a visible away, although more $E_{\mathbf{k},n}$ bands do appear, which, nevertheless, have negligible ARPES weight. As anticipated the ARPES weighted bands mostly

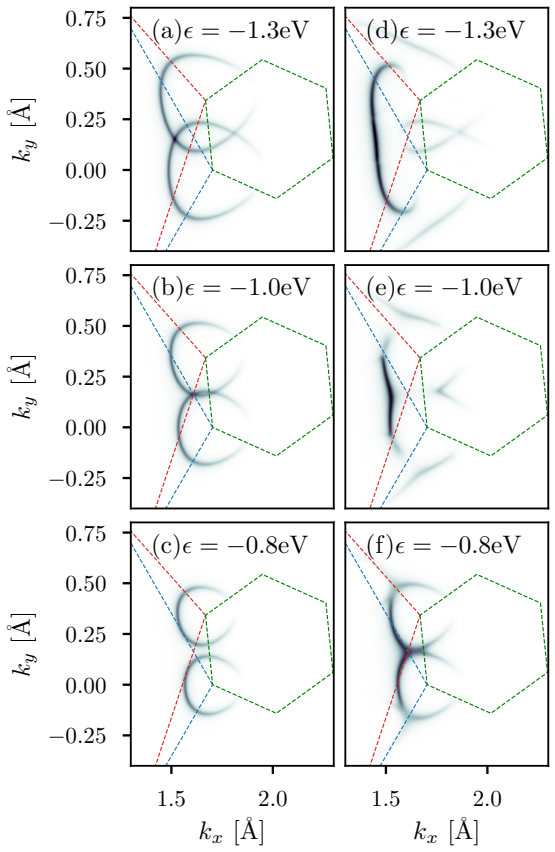

FIG. 4. Computed constant energy ARPES map for twisted bilayer graphene for a twist angle of $\theta = 11.6^\circ$ for the energies of $\epsilon = -1.3$, -1.0, and -0.8 eV measured from the Dirac point. (a)–(c) show the constant energy ARPES maps for two decoupled graphene layers, while (d)–(f) show the ARPES maps taking into account coupling between the two layers. The dashed red and blue lines show the limits of the Brillouin zone of the top and bottom layers (respectively), while the green dashed hexagon represents the moiré Brillouin zone. A broadening of $\eta = 0.05$ eV was used. The Hamiltonian was truncated with $N_G = 7$. It was assumed $Q_z = 0$.

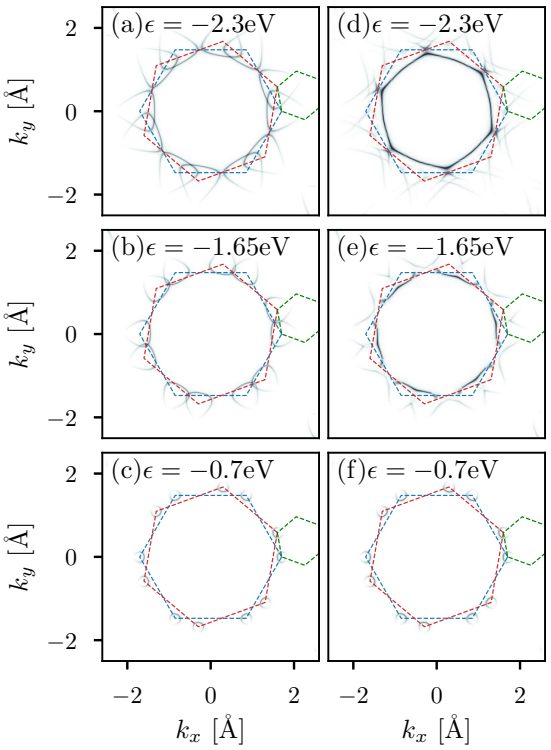

FIG. 5. Computed constant energy ARPES map for twisted bilayer graphene for a twist angle of $\theta = 20^\circ$ for the energies of $\epsilon = -2.3$, -1.65, and -0.7 eV measured from the Dirac point. (a)–(c) show the constant energy ARPES maps for two decoupled graphene layers, while (d)–(f) show the ARPES maps taking into account coupling between the two layers. The dashed red, blue, and green lines represent the same as in Fig. 4. A broadening of $\eta = 0.05$ eV was used. The Hamiltonian was truncated with $N_G = 7$. It was assumed $Q_z = 0$.

follow the bands of the decoupled system. Constant energy ARPES maps were also computed for the energies signaled by the dot-dashed horizontal lines in Fig. 3. The computed constant energy maps are shown in Figs. 4 (for $\theta = 11.6^\circ$) and 5 (for $\theta = 20^\circ$). For comparison, we also show the constant energy maps for the decoupled bilayer structures. The absence of part of the constant energy surface, due to the ARPES matrix elements, in both the coupled and decoupled cases is clear. A significant reconstruction of the constant energy ARPES maps is observed for energies at which the band structures of the isolated graphene layers intersect.

Good qualitative agreement between our results for the twist angle of $\theta = 11.6^\circ$ and the experimental data of Ref. [61] is observed, especially taking into account the simplicity of our model. There is however an observed discrepancy between our results and the experimental data: in Ref. [61] two bands are observed with energy $\simeq -1$ eV along the line that bisects the angle between the Dirac points of the two layers (Fig. 2(d) of Ref. [61]), which is shown as the path $\Gamma_m \to \mathrm{M}_m \to \Gamma_m$ in Fig. 1, while in our model there is only one band with ARPES weight around that energy. The absence of one of the ARPES bands in our results is easily understandable: the two bands are formed by bands of the top and bottom layers which are degenerate for the decoupled system along the path $\Gamma_m \to \mathrm{M}_m \to \Gamma_m$ (see the merging of two bands of the decoupled system along that line in Fig. 3) corresponding, therefore, to bonding and antibonding states. For the antibonding state we can check numerically that $\phi^{\mathrm{anti}}_{b,\mathbf{k},A}(\mathbf{0}) = -\phi^{\mathrm{anti}}_{t,\mathbf{k},B}(\mathbf{0})$ and $\phi^{\mathrm{anti}}_{b,\mathbf{k},B}(\mathbf{0}) = -\phi^{\mathrm{anti}}_{t,\mathbf{k},A}(\mathbf{0})$ [62]. For $Q_z = 0$, we then obtain $\mathcal{M}_{\mathbf{k},0,\mathrm{anti}} \propto \phi^{\mathrm{anti}}_{t,\mathbf{k},A}(\mathbf{0}) + \phi^{\mathrm{anti}}_{t,\mathbf{k},B}(\mathbf{0}) + \phi^{\mathrm{anti}}_{b,\mathbf{k},A}(\mathbf{0}) + \phi^{\mathrm{anti}}_{b,\mathbf{k},B}(\mathbf{0}) = 0$, and therefore this band would not be visible in ARPES. There are two possible explanations for the fact that the antibonding band is visible experimentally in ARPES: (i) a possible energy imbalance between the two layers, (ii) effects of finite transferred momentum along the out-of-plane direction, Q_z. As a matter of fact, a shift in energy between the Dirac cones of the two layers of $\Delta E = 0.05$ eV is reported in Ref. [61]. We have checked that this shift in energy indeed leads to $\mathcal{M}_{\mathbf{k},0,\mathrm{anti}} \neq 0$, but the value is too small to lead to a significant visibility of the antibonding band. The remaining possibility is finite-Q_z effects. For finite Q_z, we would obtain (assuming the Dirac points of both layers are

aligned)

$$\begin{aligned}\mathcal{M}_{\mathbf{k},Q_z,\text{anti}} &\propto e^{-iQ_z d}\left[\phi^{\text{anti}}_{t,\mathbf{k},A}(\mathbf{0})+\phi^{\text{anti}}_{t,\mathbf{k},B}(\mathbf{0})\right]\\ &\quad+\phi^{\text{anti}}_{b,\mathbf{k},A}(\mathbf{0})+\phi^{\text{anti}}_{b,\mathbf{k},B}(\mathbf{0})\\ &= e^{-iQ_z d/2}2\sin(Q_z d/2)\left[\phi^{\text{anti}}_{b,\mathbf{k},B}(\mathbf{0})+\phi^{\text{anti}}_{b,\mathbf{k},A}(\mathbf{0})\right],\end{aligned} \tag{61}$$

while for the bonding state, for which $\phi^{\text{bond}}_{b,\mathbf{k},A}(\mathbf{0})=\phi^{\text{bond}}_{t,\mathbf{k},B}(\mathbf{0})$ and $\phi^{\text{bond}}_{b,\mathbf{k},B}(\mathbf{0})=\phi^{\text{bond}}_{t,\mathbf{k},A}(\mathbf{0})$, we would obtain

$$\mathcal{M}_{\mathbf{k},Q_z,\text{bond}} \propto e^{-iQ_z d/2}2\cos(Q_z d/2)\left[\phi^{\text{anti}}_{b,\mathbf{k},A}(\mathbf{0})+\phi^{\text{anti}}_{b,\mathbf{k},B}(\mathbf{0})\right]. \tag{62}$$

Therefore, both bands can have similar visibility in ARPES if $Q_z d/2 \simeq (1+2n)\pi/4$, $n\in\mathbb{N}$. Besides this effect, we also expect that a better agreement with the experimental data would be possible, provided a more accurate modeling of the band structure of the individual layers was employed.

B. ARPES of twisted bilayer MoS_2

Similarly to graphene, monolayer MoS_2 has a honeycomb structure, with the A sites occupied by Mo atoms and the B sites occupied by two S atoms, top and bottom, which lie at planes above and below the Mo plane. We write the Bravais basis vectors for MoS_2 in the same way as for graphene, Eqs. (49) and (50), with a lattice constant $a\simeq 3.16$Å [63]. For an unrotated layer, the Mo and S atoms occupy the approximate positions inside the unit cell

$$\boldsymbol{\tau}_{\text{Mo}}=(0,0), \tag{63}$$

$$\boldsymbol{\tau}_{\text{S}^{\text{top/bot}}}=a\left(\frac{1}{\sqrt{3}},\pm\frac{1}{2}\right). \tag{64}$$

For the separation between the two MoS_2 layers (between the Mo planes) we use the value for bulk MoS_2 $c'\simeq 6.14$Å, which corresponds to a separation between nearest S planes of $d\simeq 2.98$AA. We will describe the electronic properties of the individual MoS_2 layers, using the 11-band tight-binding Hamiltonian of Ref. [63], with the parametrization of Ref. [64], which involves the $d_{x^2-y^2}$, d_{xy} d_{xz}, d_{yz}, d_{z^2} Mo orbitals (corresponding to the real spherical harmonics $\mathcal{Y}^2_2$, $\mathcal{Y}^{-2}_2$ $\mathcal{Y}^1_2$, $\mathcal{Y}^{-1}_2$, $\mathcal{Y}^0_2$) and the p_x, p_y, p_z S orbitals (corresponding to the real spherical harmonics $\mathcal{Y}^1_1$, $\mathcal{Y}^{-1}_1$, $\mathcal{Y}^0_1$). The Hamiltonian for an unrotated layer is given by

$$H=\sum_{n=0}^{6}\boldsymbol{c}^\dagger_{\mathbf{R}+\mathbf{a}_n}\cdot\boldsymbol{h}_n\cdot\boldsymbol{c}_{\mathbf{R}}, \tag{65}$$

where

$$\begin{aligned}\boldsymbol{c}^\dagger_{\mathbf{R}}=(&c^\dagger_{\mathbf{R},d_{x^2-y^2}},c^\dagger_{\mathbf{R},d_{xy}},c^\dagger_{\mathbf{R},d_{xz}},c^\dagger_{\mathbf{R},d_{yz}},c^\dagger_{\mathbf{R},d_{z^2}},\\ &c^\dagger_{\mathbf{R},p_x^{\text{top}}},c^\dagger_{\mathbf{R},p_y^{\text{top}}},c^\dagger_{\mathbf{R},p_z^{\text{top}}},c^\dagger_{\mathbf{R},p_x^{\text{bot}}},c^\dagger_{\mathbf{R},p_y^{\text{bot}}},c^\dagger_{\mathbf{R},p_z^{\text{bot}}})\end{aligned} \tag{66}$$

is a vector of creation operators, $\boldsymbol{h}_n$ are hoping matrices, and $\mathbf{a}_n$ are given by $\mathbf{a}_n=R(\pi(n-1)/3)\cdot\mathbf{a}_1$ for $n=1,\ldots,6$ and $\mathbf{a}_0=(0,0)$. Writing the electronic creation and annihilation operators in terms of Fourier components as in Eq. (4) we obtain the following Hamiltonian matrix in $\mathbf{k}$ space, $\boldsymbol{h}(\mathbf{k})$, with entries $h_{\alpha\beta}(\mathbf{k})=\sum_{n=0}^{6}[\boldsymbol{h}_n]_{\alpha\beta}e^{-i\mathbf{k}\cdot(\mathbf{a}_n+\boldsymbol{\tau}_\alpha-\boldsymbol{\tau}_\beta)}$, with $\alpha,\beta=d_{x^2-y^2},\ldots,p_z^{\text{bot}}$. As in the case of graphene, we will keep the bottom layer fixed, while rotating the top layer by an angle θ. When describing a MoS_2 layer rotated by an angle θ, it is important to take into account that under the rotation the orbitals will transform in a nontrivial way (in graphene this does not happen as p_z orbitals are invariant under rotations around the z axis). We chose to represent the Hamiltonian of both layers in terms of orbitals defined with respect to the same common reference frame, which we choose to be the unrotated frame. It is also with respect to this common reference frame that the plane wave expansion Eq. (40) is written. Taking this into account, we can write the Hamiltonian matrix for each layer, in the orbital basis defined with respect to the common reference frame, as

$$\boldsymbol{h}^{b,b}_{\mathbf{k}}=\boldsymbol{h}(\mathbf{k}), \tag{67}$$

$$\boldsymbol{h}^{t,t}_{\mathbf{k}}=\boldsymbol{\mathcal{R}}(\theta)\cdot\boldsymbol{h}[R(-\theta)\cdot\mathbf{k}]\cdot\boldsymbol{R}(-\theta), \tag{68}$$

where the matrix $\boldsymbol{\mathcal{R}}(\theta)$ rotates the orbitals in Eq. (66) along the z axis, and has the block diagonal form

$$\boldsymbol{\mathcal{R}}(\theta)=\begin{bmatrix}R(2\theta) & & & & & \\ & R(\theta) & & & & \\ & & 1_{1\times1} & & & \\ & & & R(\theta) & & \\ & & & & 1_{1\times1} & \\ & & & & & R(\theta) \\ & & & & & & 1_{1\times1}\end{bmatrix}, \tag{69}$$

with $R(\theta)$ the rotation matrix Eq. (53). For the interlayer coupling, we assume that this is dominated by the hopping between the S^{top} p orbitals of the bottom MoS_2 layer and the S^{bot} p orbitals of the MoS_2 layer. We write the interlayer hoppings in terms of Slater-Koster parameters as

$$\begin{aligned}h^{tb}_{p_i^{\text{bot}},p_j^{\text{top}}}(\mathbf{r})&=h^{tb}_{p_i^{\text{bot}},p_j^{\text{top}}}(\mathbf{r},d)\\ &=V_{pp\sigma}(R)\frac{R^iR^j}{R^2}+V_{pp\pi}(R)\left(\delta_{ij}-\frac{R^iR^j}{R^2}\right),\\ i,j&=x,y,z,\end{aligned} \tag{70}$$

where $\mathbf{R}=(x,y,d)$ is the separation between the S atoms. As before, we assume a dependence of the Slater-Koster parameters on the distance of the form $V_{pp\sigma}(R)=V^0_{pp\sigma}e^{-\beta(R/d_{SS}-1)}$ and $V_{pp\pi}(R)=V^0_{pp\pi}e^{-\beta(R/d_{SS}-1)}$. We use $V^0_{pp\sigma}\simeq-0.774$ eV and $V^0_{pp\pi}\simeq 0.123$ eV, which are the interlayer hoppings used in Ref. [63], with $d_{SS}\simeq 3.49$Å the interlayer nearest-neighbor separation between S atoms in bulk MoS_2. In the absence of *ab initio* calculations, we assume the value $\beta\simeq 3$, in accordance with Harrison's argument [65] and as previously used to model strained MoS_2 [66]. The Fourier transform of $h^{tb}_{p_i^{\text{bot}},p_j^{\text{top}}}(\mathbf{r},d)$ can

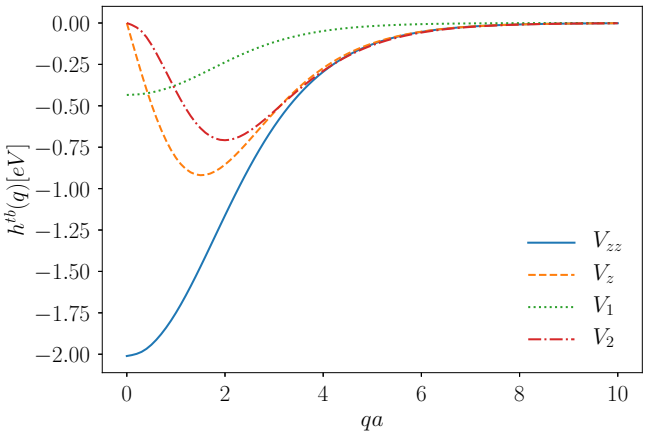

FIG. 6. Plot of the interlayer coupling functions $V_{zz}(q)$, $V_z(q)$, $V_1(q)$, and $V_2(q)$ for bilayer MoS_2, Eq. (71), as a function of qa, with a the lattice parameter of MoS_2. The parameters used are given in the main text.

be written as

$$h^{tb}_{p_i^{\rm bot},p_j^{\rm top}}(\mathbf{q}) = \begin{bmatrix} V_1(q)-\frac{q_x^2}{q^2}V_2(q) & -\frac{q_xq_y}{q^2}V_2(q) & -i\frac{q_x}{q}V_z(q) \\ -\frac{q_xq_y}{q^2}V_2(q) & V_1(q)-\frac{q_y^2}{q^2}V_2(q) & -i\frac{q_y}{q}V_z(q) \\ -i\frac{q_x}{q}V_z(q) & -i\frac{q_y}{q}V_z(q) & V_{zz}(q) \end{bmatrix}, \tag{71}$$

where the functions $V_{zz}(q)$, $V_z(q)$, $V_1(q)$, and $V_2(q)$ are shown in Fig. 6 and the explicit expressions used to evaluate them are provided in Appendix B. We point out that the general expression for $V_{zz}(q)$ is the same as for graphene, Eq. (58). As for graphene, we can see that the Fourier components of the interlayer hoppings decay fast. Having evaluated $h^{tb}_{p_i^{\rm bot},p_j^{\rm top}}(\mathbf{q})$ we can construct the matrices $\boldsymbol{h}^{t,b}_{\mathbf{k},\mathbf{G}_b,\mathbf{G}_t}$ and $\boldsymbol{h}^{b,t}_{\mathbf{k},\mathbf{G}_t,\mathbf{G}_b}$, from which, together with Eqs. (67) and (68), we can build the Hamiltonian matrix for the twisted bilayer according to Eqs. (12)–(14). Keeping the N_G shortest $\mathbf{G}_t$ and $\mathbf{G}_b$ vectors, $\boldsymbol{H}_{\mathbf{k}}(\{\mathbf{G}_b\},\{\mathbf{G}_t\})$ becomes an $11N_G \times 11N_G$ matrix, from which the energies and eigenstates of twisted bilayer MoS_2 can be evaluated and then used to model the ARPES intensity. As already pointed out, the tight-binding model for MoS_2 involves orbitals that do not transform trivially under rotations around the z axis. Therefore, it is essential to keep the factors $\Phi_{m_\alpha}(\phi_{\hat{\mathbf{Q}}})$, Eq. (39), in the ARPES matrix element $\mathcal{M}_{\mathbf{Q},n}$ in order to obtain an ARPES signal that respects the threefold rotational invariance of the twisted bilayer MoS_2 structure.

In Fig. 7 we show the computed ARPES bands and constant energy maps for a twisted bilayer MoS_2 with a twist angle of $\theta = 13.5°$, for which ARPES measurements have been performed [67]. The calculations where performed truncating the Hamiltonian matrix with $N_G = 7$. As can be seen in Fig. 7(a), by comparing with the bands of the decoupled layers, the interlayer coupling leads to a large splitting of the states at the Γ point, with one of them becoming the valence band maximum. This also occurs for bulk MoS_2 [63] and has been predicted by *ab initio* calculations for commensurate twisted

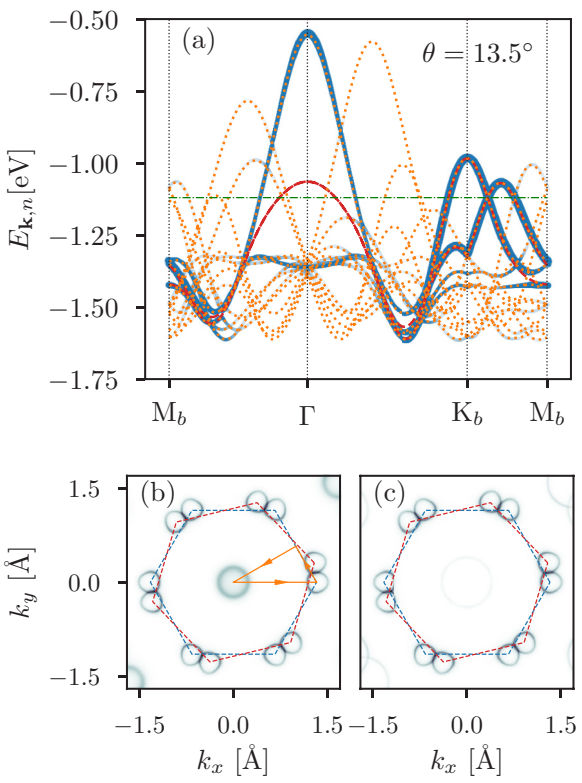

FIG. 7. Computed ARPES bands, (a), and constant energy map, (b) and (c), for twisted bilayer MoS_2 for a twist angle of $\theta = 13.5°$. In (a), the bands are computed along the path $M_b \to \Gamma \to K_b \to M_b$ [shown in (b)]. The yellow dotted lines show the band structure, $E_{\mathbf{k},n}$, while the blue tick bands represent $E_{\mathbf{k},n}$ weighted by the ARPES matrix element value, with the thickness corresponding to $|\mathcal{M}_{\mathbf{k},0,n}|^2$. The dashed red lines show the band structure for the decoupled MoS_2 layers. The horizontal dot-dashed green line marks the energy $\epsilon = -1.12$ eV, at which the constant energy maps (b) and (c) are computed. (b) and (c) are, respectively, the constant energy maps for decoupled and coupled twisted bilayer MoS_2. A broadening of $\eta = 0.02$ eV was used. The Hamiltonian for the coupled bilayer structure was truncated with $N_G = 7$. In all plots it was assumed $Q_z = 0$.

bilayer structures for several twist angles [67–69]. We checked that if the interlayer distance is kept fixed, this splitting at Γ is virtually independent of the twist angle. From this, it can be inferred that the change in the splitting at Γ with angle predicted in [67–69] and observed in the ARPES measurements of [67] is due to the interlayer separation modulation with the twist angle, which we kept fixed. As we can see in Fig. 7(a), the effect of the interlayer coupling is negligible at the K point. As in the case of twisted bilayer graphene, the backfolded bands have negligible visibility in ARPES. In Fig. 7(c), we show the constant energy map for the same $\theta = 13.5°$ twist angle. For comparison, the ARPES constant energy map for the decoupled layer is shown in Fig. 7(b). Once again, it can be seen that the interlayer coupling affects more strongly the states close to the Γ point having almost no impact on the states close to the K points. It is observed that the valence band pocket at the Γ point has very weak visibility in ARPES in agreement with what is experimentally observed in Ref. [67].

V. CONCLUSIONS

In this work we developed a general theoretical framework to model ARPES of lattice mismatch/misaligned vdW structures. By describing the photoemitted state as a plane wave and the bound electronic states in terms of Bloch waves of the individual layers, while taking into account generalized umklapp processes, we obtained an efficient description of ARPES that can be applied both to commensurate and incommensurate structures. Being based on a tight-binding description of the bound electronic states, the present formalism can deal with arbitrary lattice mismatch/misalignment, going beyond previous low-energy, continuum descriptions of both twisted bilayer graphene and graphene/h-BN structures. We applied the developed formalism to the cases of twisted bilayer graphene and twisted bilayer MoS_2. The example of graphene showcases the importance of the ARPES matrix elements in two ways: (i) by showing the importance of the momentum dependence of the ARPES weight in entangled bands, which is responsible for the absence of part of the constant energy surface map around the K points, and (ii) by showing that the ARPES weight of backfolded bands is very small, which is a consequence of the weak coupling between the two layers. As a consequence, the observed ARPES bands mostly follow the band structure of the decoupled system, except at energies at which states from both layers are degenerate, where a significant reconstruction of the spectrum occurs. By comparing the results of the current model to the experimental data of ARPES of twisted bilayer graphene at a twist angle $\theta = 11.6^\circ$ [61], we showcased the importance of the transferred momentum between the incoming radiation and the photoemitted state along the z direction, which significantly affects the visibility of bands in ARPES that correspond to bonding and antibonding states of the two layers. In the example of MoS_2, we once again observed that the ARPES bands mostly follow the band structure of the decoupled system. Differently from graphene, we found out that while there is a significant shift in energy of the states at the Γ point, the reconstruction of the valence band close to the K points due to the interlayer coupling is negligible, which is in accordance with experimental ARPES data [67].

Although this work focused on bilayer vdW structures, the formalism can also be applied to structures formed by multiple lattice misaligned/mismatch layers. We would like to point out that the present approach to model ARPES can also be extended to other systems where competition between different periodicities occurs, both commensurate and incommensurate, such as 2D materials placed on top of a weakly coupled substrate or materials displaying CDW phases. The coupling to a substrate can be described via a substrate surface Green's function, which would play a role similar to H_b in the present work. The effect of the substrate can also be approximated by a potential which acts on the 2D material. In systems with CDW phases, two cases must be distinguished: (i) a system with weak fluctuations, which can be described at a single-particle level, and (ii) a strongly interacting system, with strong fluctuations. In the former case, it is possible to describe the system with a single-particle (mean-field) Hamiltonian as done in this work. In the latter case, it is not possible to describe the system at a single-particle level and the electronic spectral function of crystal bound states, which can be severely reconstructed by the interactions, has to be obtained from the full Green's function of the interacting system [52]. In this case, it is therefore crucial to distinguish between the effects of interactions and the effects of the ARPES matrix elements (which encode the effect of competition between the different periodicities) [13]. The approach presented in this work can be used to take into account the latter effect.

ACKNOWLEDGMENTS

The author would like to acknowledge useful discussions with J. L. Lado, J. Fernández-Rossier, and Eduardo V. Castro. The author also acknowledges the hospitality of the International Iberian Nanotechnology Laboratory (INL), where early ideas on this problem were developed. B.A. received funding from the European Union's Horizon 2020 research and innovation program under Grant Agreement No. 706538.

APPENDIX A: NONEQUILIBRIUM GREEN'S FUNCTION DESCRIPTION OF ARPES

In this Appendix we briefly review the rigorous derivation of the observed photoemitted current in an ARPES experiment using the nonequilibrium Green's function technique. This approach was first developed in Ref. [31] and its connection to other formalisms and experimental observations clarified in Ref. [32].

In order to describe the process of photoemission, we must consider both states that are bound to the crystal and unbound, nearly free states. Therefore, in the model employed, the crystal must not occupy the entire space. For concreteness we assume that the positions of the atoms that form the crystal are restricted to the $z \leqslant 0$ region. We assume that the crystal is infinite along the x-y plane. The single-particle Hamiltonian for the electrons reads

$$H_0 = \int d^3\mathbf{r}\Psi^\dagger(\mathbf{r})\left[\frac{\mathbf{p}^2}{2m} + V(\mathbf{r})\right]\Psi(\mathbf{r}), \tag{A1}$$

where $\Psi^\dagger(\mathbf{r})$ is the electronic creation field operator, $V(\mathbf{r})$ is the crystal potential, and $\mathbf{p} = -i\hbar\nabla_{\mathbf{r}}$. We describe the exciting electromagnetic field in the Weyl gauge, such that $\mathbf{E}(t,\mathbf{r}) = -\partial_t\mathbf{A}(t,\mathbf{r})$ and $\mathbf{B}(t,\mathbf{r}) = \nabla \times \mathbf{A}(t,\mathbf{r})$, where $\mathbf{A}(t,\mathbf{r})$ is the vector potential. The coupling to the electromagnetic field is obtained via minimal coupling $\mathbf{p} \to \mathbf{p} + e\mathbf{A}(t,\mathbf{r})$. In the presence of the vector potential, the Hamiltonian can be written as the sum of three terms

$$H = H_0 + H_{1,\mathbf{A}} + H_{2,\mathbf{A}}, \tag{A2}$$

where H_0 is the same as in Eq. (A1) and

$$H_{1,\mathbf{A}} = -\int d^3\mathbf{r}[\Psi^\dagger(\mathbf{r})\mathbf{J}^{(1)}(\mathbf{r})\Psi(\mathbf{r})] \cdot \mathbf{A}(\mathbf{r},t), \tag{A3}$$

$$H_{2,\mathbf{A}} = -\frac{1}{2}\int d^3\mathbf{r}[\Psi^\dagger(\mathbf{r})J^{(2)}(\mathbf{r})\Psi(\mathbf{r})]\mathbf{A}^2(\mathbf{r},t), \tag{A4}$$

with

$$\mathbf{J}^{(1)}(\mathbf{r}) = -\frac{e\hbar}{2mi}(\overrightarrow{\nabla}_{\mathbf{r}} - \overleftarrow{\nabla}_{\mathbf{r}}), \tag{A5}$$

$$J^{(2)}(\mathbf{r}) = -\frac{e^2}{m}, \tag{A6}$$

the matrix elements in real space of the paramagnetic and diamagnetic currents, respectively. The arrows in the differential operator indicate whether the derivative acts on the electronic field operator placed to the right or to the left. The expectation value of the current is given by

$$\langle \mathbf{J}(t,\mathbf{r})\rangle = \lim_{\mathbf{r}'\to\mathbf{r}}\left[-e\frac{\hbar}{2mi}(\nabla_{\mathbf{r}}-\nabla_{\mathbf{r}'})-\frac{e^2}{m}\mathbf{A}(t,\mathbf{r})\right] \times(-i)G^{<}_{\mathbf{A}}(t,\mathbf{r};t,\mathbf{r}'), \tag{A7}$$

with the lesser Green's function defined as

$$G^{<}_{\mathbf{A}}(t,\mathbf{r};t',\mathbf{r}') = i\langle\Psi^{\dagger}(t',\mathbf{r}')\Psi(t,\mathbf{r})\rangle_{\mathbf{A}}, \tag{A8}$$

where the $\mathbf{A}$ subscript means the expectation value is evaluated taking into account $\mathbf{A}(t,\mathbf{r})$. This can be done perturbatively in $\mathbf{A}(t,\mathbf{r})$ using the nonequilibrium Green's function formalism [70,71]. By expanding the contour-ordered Green's function in the Schwinger-Keldysh contour in powers of $\mathbf{A}(t,\mathbf{r})$ and then using Langreth's rules, the lesser Green's function is given to second order in $\mathbf{A}(t,\mathbf{r})$ by

$$\begin{aligned}\boldsymbol{G}^{<}_{\mathbf{A}} &= \boldsymbol{G}^{<}+\boldsymbol{G}^{<}\odot(\mathbf{J}^{(1)}\cdot\mathbf{A})\odot\boldsymbol{G}^{A}\\ &+\boldsymbol{G}^{R}\odot(\mathbf{J}^{(1)}\cdot\mathbf{A})\odot\boldsymbol{G}^{<}\\ &+\frac{1}{2}\boldsymbol{G}^{<}\odot(J^{(2)}\mathbf{A}^2)\odot\boldsymbol{G}^{A}\\ &+\frac{1}{2}\boldsymbol{G}^{R}\odot(J^{(2)}\mathbf{A}^2)\odot\boldsymbol{G}^{<}\\ &+\boldsymbol{G}^{<}\odot(\mathbf{J}^{(1)}\cdot\mathbf{A})\cdot\boldsymbol{G}^{A}\cdot(\mathbf{J}^{(1)}\cdot\mathbf{A})\odot\boldsymbol{G}^{A}\\ &+\boldsymbol{G}^{R}\odot(\mathbf{J}^{(1)}\cdot\mathbf{A})\odot\boldsymbol{G}^{R}\odot(\mathbf{J}^{(1)}\cdot\mathbf{A})\odot\boldsymbol{G}^{<}\\ &+\boldsymbol{G}^{R}\odot(\mathbf{J}^{(1)}\cdot\mathbf{A})\odot\boldsymbol{G}^{<}\odot(\mathbf{J}^{(1)}\cdot\mathbf{A})\odot\boldsymbol{G}^{A}\\ &+\mathcal{O}(\mathbf{A}^3),\end{aligned} \tag{A9}$$

where the retarded and advanced Green's functions are given by

$$G^{R}(t,\mathbf{r};t',\mathbf{r}') = -i\Theta(t-t')\langle\{\Psi(t,\mathbf{r}),\Psi^{\dagger}(t',\mathbf{r}')\}\rangle, \tag{A10}$$

$$G^{A}(t,\mathbf{r};t',\mathbf{r}') = i\Theta(t'-t)\langle\{\Psi(t,\mathbf{r}),\Psi^{\dagger}(t',\mathbf{r}')\}\rangle, \tag{A11}$$

and the $\odot$ product represents integration over the spatial variables and time, and summation over other possible degrees of freedom (sublattice, orbital, spin, ...). All the Green's functions in Eq. (A9) are evaluated in the absence of $\mathbf{A}(t,\mathbf{r})$, and are therefore in thermodynamic equilibrium. In Eq. (A9) interactions between the emitted state and the remaining hole are neglected, an approximation that is typically referred to as the sudden approximation. Including these kinds of interactions would lead to a renormalization of the vertices $\mathbf{J}^{(1)}$ and $J^{(2)}$ [31]. For a photodectector placed very far away from the crystal sample, only the last term in Eq. (A9) gives a finite contribution. This can be understood if we write $G^{<}$ in terms of the eigenstates $\psi_a(\mathbf{r})$ of Eq. (A1). The creation field operator can be written as $\Psi^{\dagger}(\mathbf{r}) = \sum_a c_a^{\dagger}\psi_a^{*}(\mathbf{r})$, where $c_a^{\dagger}$ creates an electron in state $\psi_a(\mathbf{r})$ with energy ϵ_a, and the lesser Green's function, for a noninteracting system, becomes

$$G^{<}(t,\mathbf{r};t',\mathbf{r}') = \sum_a \psi_a(\mathbf{r})\psi_a^{*}(\mathbf{r}')e^{-i\epsilon_a(t-t')}i\langle c_a^{\dagger}c_a\rangle. \tag{A12}$$

Notice that only crystal bound states are occupied, and therefore the sum in previous equations is restricted to those states due to the occupation function $\langle c_a^{\dagger}c_a\rangle$. At the same time, the wave function of crystal bound states decays exponentially away from the crystal. Therefore if one of the arguments of $G^{<}$ is evaluated away from the crystal, that term can be safely neglected. This also allows us to discard the diamagnetic term in Eq. (A7), as it would only contribute to third order in $\mathbf{A}(t,\mathbf{r})$. Therefore, to second order in the electromagnetic field, the photoemitted current measured away from the crystal is given by

$$\begin{aligned}\langle \mathbf{J}(t,\mathbf{r})\rangle &= \lim_{\mathbf{r}'\to\mathbf{r}}\frac{e\hbar}{2m}(\nabla_{\mathbf{r}}-\nabla_{\mathbf{r}'})\int dt_1 d^3\mathbf{r}_1\int dt_2 d^3\mathbf{r}_2\\ &\times G^{R}(t,\mathbf{r};t_1,\mathbf{r}_1)\mathbf{J}^{(1)}(\mathbf{r}_1)\cdot\mathbf{A}(t_1,\mathbf{r}_1)\\ &\times G^{<}(t_1,\mathbf{r}_1;t_2,\mathbf{r}_2)\mathbf{J}^{(1)}(\mathbf{r}_2)\cdot\mathbf{A}(t_2,\mathbf{r}_2)G^{A}(t_2,\mathbf{r}_2;t,\mathbf{r}').\end{aligned} \tag{A13}$$

Assuming a monochromatic electromagnetic field at frequency $\omega_0 > 0$,

$$\mathbf{A}(t,\mathbf{r}) = \mathbf{A}_{\omega_0}(\mathbf{r})e^{-i\omega_0 t}+\mathbf{A}_{-\omega_0}(\mathbf{r})e^{i\omega_0 t}, \tag{A14}$$

expressing all quantities in Fourier components in time and looking at the time-averaged current over one period $2\pi/\omega_0$, we obtain

$$\begin{aligned}\overline{\langle \mathbf{J}(\mathbf{r})\rangle} &= \lim_{\mathbf{r}'\to\mathbf{r}}\frac{e\hbar}{2m}(\nabla_{\mathbf{r}}-\nabla_{\mathbf{r}'})\int\frac{dE}{2\pi}\int d^3\mathbf{r}_1\int d^3\mathbf{r}_2\\ &\times\big[G^{R}(E;\mathbf{r},\mathbf{r}_1)\mathbf{J}^{(1)}(\mathbf{r}_1)\cdot\mathbf{A}_{\omega_0}(\mathbf{r}_1)G^{<}(E-\omega_0;\mathbf{r}_1,\mathbf{r}_2)\\ &\times\mathbf{J}^{(1)}(\mathbf{r}_2)\cdot\mathbf{A}_{-\omega_0}(\mathbf{r}_2)G^{A}(E;\mathbf{r}_2,\mathbf{r}')+(\omega_0\leftrightarrow-\omega_0)\big].\end{aligned} \tag{A15}$$

Some further simplifications can be performed. First, by using the fluctuation-dissipation theorem, which is valid in thermodynamic equilibrium even for an interacting system, we can write

$$G^{<}(E;\mathbf{r}_1,\mathbf{r}_2) = \sum_a \psi_a(\mathbf{r}_1)\psi_a^{*}(\mathbf{r}_2)if(E-\mu)\mathcal{A}_a(E), \tag{A16}$$

where $\mathcal{A}_a(E) = G_a^{R}(E) - G_a^{A}(E)$ is the electronic spectral function in the eigenstate basis, and $f(\omega) = (e^{\beta\omega}+1)^{-1}$ is the Fermi-Dirac distribution function with μ the chemical potential. Once again, only crystal bound states are occupied and therefore, the integration over the spatial coordinates in Eq. (A15) is mostly confined to the region of the crystal. This allows us to use the asymptotic expression of the retarded and advanced Green's functions, valid for $\mathbf{r}$ and $\mathbf{r}'$ far away from the crystal [32,41],

$$G^{R}(E;\mathbf{r},\mathbf{r}_1) \simeq -\frac{2m}{\hbar^2}\frac{1}{4\pi r}e^{ip_E r}\psi^{*}_{E,\hat{\mathbf{r}}}(\mathbf{r}_1), \tag{A17}$$

$$G^{A}(E;\mathbf{r}_2,\mathbf{r}') \simeq -\frac{2m}{\hbar^2}\frac{1}{4\pi r'}\psi_{E,\hat{\mathbf{r}}}(\mathbf{r}_2)e^{-ip_E^{*}r'}, \tag{A18}$$

where $p_E = \sqrt{2mE/\hbar^2}$ for $E>0$ and $p_E = i\sqrt{2m|E|/\hbar^2}$ for $E<0$ (we choose as zero of energy the threshold to have free electron states), $\psi^{*}_{E,\hat{\mathbf{r}}}(\mathbf{r}_1)$, given by Eq. (28), is the conjugate of an electron diffraction state [32,41], $\hat{\mathbf{r}}$ is the unit vector pointing along $\mathbf{r}$, and $G^{R}_{\text{free}}(E;\mathbf{r},\mathbf{r}')$ is the free space retarded Green's

function

$$G^R_{\text{free}}(E;\mathbf{r},\mathbf{r}') = -\frac{2m}{\hbar^2}\frac{1}{4\pi}\frac{e^{ip_E|\mathbf{r}-\mathbf{r}'|}}{|\mathbf{r}-\mathbf{r}'|}. \tag{A19}$$

Equation (A17) can be obtained from the Dyson equation for the retarded Green's function

$$G^R(E;\mathbf{r},\mathbf{r}') = G^R_{\text{free}}(E;\mathbf{r},\mathbf{r}') + \int d^3\mathbf{r}_1 G^R_{\text{free}}(E;\mathbf{r},\mathbf{r}_1) \times V(\mathbf{r}_1)G^R(E;\mathbf{r}_1,\mathbf{r}'). \tag{A20}$$

If we are interested in the Green's function when $\mathbf{r}$ is very far away from the crystal, we can use the following approximation for $G^R_{\text{free}}(E;\mathbf{r},\mathbf{r}')$, valid for $|\mathbf{r}| \gg |\mathbf{r}'|$,

$$G^R_{\text{free}}(E;\mathbf{r},\mathbf{r}') \simeq -\frac{2m}{\hbar^2}\frac{1}{4\pi}\frac{e^{ip_E r}}{r}e^{-ip_R\hat{\mathbf{r}}\cdot\mathbf{r}'}. \tag{A21}$$

Inserting this approximation into the Dyson equation (A20), we obtain Eq. (A17) with

$$\psi^*_{E,\hat{\mathbf{r}}}(\mathbf{r}') = e^{-ip_E\hat{\mathbf{r}}\cdot\mathbf{r}'} + \int d^3\mathbf{r}_1 e^{-ip_E\hat{\mathbf{r}}\cdot\mathbf{r}_1}V(\mathbf{r}_1)G^R(E;\mathbf{r}_1,\mathbf{r}'). \tag{A22}$$

Using the Dyson equation for the Green's function Eq. (A20), we can rewrite the above equation as Eq. (28), which is nothing more than the Lippmann-Schwinger equation for the scattering of an incoming plane wave state, $\phi^*_0(\mathbf{r}') = e^{-ip_E\hat{\mathbf{r}}\cdot\mathbf{r}'}$, by the crystal potential $V(\mathbf{r})$. Equation (A18) for the advanced Green's function can be obtained in a similar way. Inserting Eqs. (A16), (A17), and (A18) in Eq. (A15), the detected photoemitted current becomes

$$\overline{\langle\mathbf{J}(\mathbf{r})\rangle} = \frac{-e}{(4\pi r)^2}\hat{\mathbf{r}}\int\frac{dE}{2\pi}\text{Re}\left[\frac{\hbar p_E}{m}e^{i(p_E-p^*_E)r}\right] \times\sum_a\Big[f(E-\omega_0-\mu)\big|M_{E,\hat{\mathbf{r}};a}(\omega_0)\big|^2\mathcal{A}_a(E-\omega_0) + (\omega_0\leftrightarrow-\omega_0)\Big], \tag{A23}$$

where we have defined the ARPES matrix elements as

$$M_{E,\mathbf{n};a}(\omega_0) = -\frac{2m}{\hbar^2} \times\int d^3\mathbf{r}_1\big[\psi^*_{E,\mathbf{n}}(\mathbf{r}_1)\mathbf{J}^{(1)}(\mathbf{r}_1)\psi_a(\mathbf{r}_1)\big]\cdot\mathbf{A}_{\omega_0}(\mathbf{r}_1), \tag{A24}$$

which can also be written as Eq. (27) of the main text. For $E<0$, we have that $e^{i(p_E-p^*_E)r} = e^{-2|p_E|r}$ and therefore this contribution vanishes for a detector far away from the crystal. Therefore, we can restrict the integration in Eq. (A23) from 0 to $+\infty$. At the same time, we notice that the second term in Eq. (A23) involves states with energy $E+\omega_0>0$ which are unoccupied, and can therefore be neglected. This allows us to write

$$\overline{\langle\mathbf{J}(\mathbf{r})\rangle} = \frac{-e}{(4\pi r)^2}\hat{\mathbf{r}}\int_0^{+\infty}\frac{dE}{2\pi}\frac{\hbar p_E}{m}f(E-\omega_0-\mu) \times\sum_a\big|M_{E,\hat{\mathbf{r}};a}(\omega_0)\big|^2\mathcal{A}_a(E-\omega_0). \tag{A25}$$

Assuming that the electron detector can resolve the energy of the photoemitted states and it collects electrons emitted along direction $\hat{\mathbf{r}}$, the measured ARPES intensity is proportional to Eq. (26) of the main text.

APPENDIX B: FOURIER TRANSFORM OF INTERLAYER HOPPING FOR MoS_2

In this Appendix, we provide details on how the two-dimensional Fourier transform of the interlayer coupling for S p orbitals for twisted bilayer MoS_2, Eq. (70), is computed. We wish to evaluate

$$h^{tb}_{p_i^{\text{bot}},p_j^{\text{top}}}(\mathbf{q}) = \int\frac{d^2\mathbf{r}}{A_c}e^{-i\mathbf{q}\cdot\mathbf{r}}\times \begin{bmatrix} v_1(r)+v_2(r)\frac{x^2}{R^2} & v_2(r)\frac{xy}{R^2} & v_2(r)\frac{xd}{R^2} \\ v_2(r)\frac{xy}{R^2} & v_1(r)+v_2(r)\frac{y^2}{R^2} & v_2(r)\frac{yd}{R^2} \\ v_2(r)\frac{xd}{R^2} & v_2(r)\frac{yd}{R^2} & v_1(r)+v_2(r)\frac{d^2}{R^2}\end{bmatrix}, \tag{B1}$$

where $v_1(r) = V_{pp\pi}(R)$ and $v_2(r) = V_{pp\sigma}(R) - V_{pp\pi}(R)$, with $R=\sqrt{r^2+d^2}$, and A_c is the unit cell area of MoS_2. We have three kinds of integrals:

$$\mathcal{I}_0(\mathbf{q}) = \int d^2\mathbf{r}e^{-i\mathbf{q}\cdot\mathbf{r}}f(r), \tag{B2}$$

$$\mathcal{I}_i(\mathbf{q}) = \int d^2\mathbf{r}e^{-i\mathbf{q}\cdot\mathbf{r}}x_i f(r), \tag{B3}$$

$$\mathcal{I}_{ij}(\mathbf{q}) = \int d^2\mathbf{r}e^{-i\mathbf{q}\cdot\mathbf{r}}x_i x_j f(r), \tag{B4}$$

where $f(r)$ is a function only of $r=|\mathbf{r}|$. Using the fact that $\int_0^{2\pi}d\phi e^{-ix\cos\phi} = 2\pi J_0(x)$, where $J_0(x)$ is the Bessel function of first kind and order 0, we can write

$$\mathcal{I}_0(\mathbf{q}) = 2\pi\int drrf(r)J_0(qr). \tag{B5}$$

The integrals $\mathcal{I}_i(\mathbf{q})$ and $\mathcal{I}_{ij}(\mathbf{q})$ can be written as

$$\mathcal{I}_i(\mathbf{q}) = i\int d^2\mathbf{r}\left(\frac{\partial}{\partial q_i}e^{-i\mathbf{q}\cdot\mathbf{r}}\right)f(r) = i\int drrf(r)\frac{\partial}{\partial q_i}J_0(qr), \tag{B6}$$

$$\mathcal{I}_{ij}(\mathbf{q}) = -\int d^2\mathbf{r}\left(\frac{\partial^2}{\partial q_i\partial q_j}e^{-i\mathbf{q}\cdot\mathbf{r}}\right)f(r) = -\int drrf(r)\frac{\partial^2}{\partial q_i\partial q_j}J_0(qr). \tag{B7}$$

Using the properties of Bessel functions, it is possible to write

$$\frac{\partial}{\partial q_i}J_0(qr) = -\frac{1}{2}r^2q_i[J_0(qr)+J_2(qr)], \tag{B8}$$

$$\frac{\partial^2}{\partial q_i\partial q_j}J_0(qr) = -\delta_{ij}\frac{1}{2}r^2[J_0(qr)+J_2(qr)] + \frac{q_iq_j}{q^2}r^2J_2(qr). \tag{B9}$$

Using this, we can write Eq. (B1) as Eq. (71), with

$$V_1(q) = \frac{2\pi}{A_c}\int drr\Big[v_1(r)J_0(qr) + \frac{1}{2}v_2(r)\frac{r^2}{R^2}[J_0(qr)+J_2(qr)]\Big], \quad \text{(B10)}$$

$$V_2(q) = \frac{2\pi}{A_c}\int drrv_2(r)\frac{r^2}{R^2}J_2(qr), \quad \text{(B11)}$$

$$V_z(q) = qd\frac{\pi}{A_c}\int drrv_2(r)\frac{r^2}{R^2}[J_0(qr)+J_2(qr)], \quad \text{(B12)}$$

$$V_{zz}(q) = \frac{2\pi}{A_c}\int drr\Big[v_1(r)+v_2(r)\frac{d^2}{R^2}\Big]J_0(qr). \quad \text{(B13)}$$

The remaining integration over r has to be performed numerically.

[1] L. A. Ponomarenko, A. K. Geim, A. A. Zhukov, R. Jalil, S. V. Morozov, K. S. Novoselov, I. V. Grigorieva, E. H. Hill, V. V. Cheianov, V. I. Fal'ko, K. Watanabe, T. Taniguchi, and R. V. Gorbachev, Nat. Phys. **7**, 958 (2011).

[2] K. S. Novoselov and A. H. C. Neto, Phys. Scr. **2012**, 014006 (2012).

[3] A. K. Geim and I. V. Grigorieva, Nature (London) **499**, 419 (2013).

[4] L. Britnell, R. V. Gorbachev, R. Jalil, B. D. Belle, F. Schedin, A. Mishchenko, T. Georgiou, M. I. Katsnelson, L. Eaves, S. V. Morozov, N. M. R. Peres, J. Leist, A. K. Geim, K. S. Novoselov, and L. A. Ponomarenko, Science **335**, 947 (2012).

[5] T. Georgiou, R. Jalil, B. D. Belle, L. Britnell, R. V. Gorbachev, S. V. Morozov, Y.-J. Kim, A. Gholinia, S. J. Haigh, O. Makarovsky, L. Eaves, L. A. Ponomarenko, A. K. Geim, K. S. Novoselov, and A. Mishchenko, Nat. Nanotechnol. **8**, 100 (2012).

[6] L. Britnell, R. M. Ribeiro, A. Eckmann, R. Jalil, B. D. Belle, A. Mishchenko, Y.-J. Kim, R. V. Gorbachev, T. Georgiou, S. V. Morozov, A. N. Grigorenko, A. K. Geim, C. Casiraghi, A. H. C. Neto, and K. S. Novoselov, Science **340**, 1311 (2013).

[7] W. J. Yu, Y. Liu, H. Zhou, A. Yin, Z. Li, Y. Huang, and X. Duan, Nat. Nanotechnol. **8**, 952 (2013).

[8] M. Massicotte, P. Schmidt, F. Vialla, K. G. Schädler, A. Reserbat-Plantey, K. Watanabe, T. Taniguchi, K. J. Tielrooij, and F. H. L. Koppens, Nat. Nanotechnol. **11**, 42 (2016).

[9] A. Mishchenko, J. S. Tu, Y. Cao, R. V. Gorbachev, J. R. Wallbank, M. T. Greenaway, V. E. Morozov, S. V. Morozov, M. J. Zhu, S. L. Wong, F. Withers, C. R. Woods, Y.-J. Kim, K. Watanabe, T. Taniguchi, E. E. Vdovin, O. Makarovsky, T. M. Fromhold, V. I. Fal'ko, A. K. Geim, L. Eaves, and K. S. Novoselov, Nat. Nanotechnol. **9**, 808 (2014).

[10] L. Brey, Phys. Rev. Applied **2**, 014003 (2014).

[11] B. Amorim, R. M. Ribeiro, and N. M. R. Peres, Phys. Rev. B **93**, 235403 (2016).

[12] A. Damascelli, Z. Hussain, and Z.-X. Shen, Rev. Mod. Phys. **75**, 473 (2003).

[13] A. A. Kordyuk, Low Temp. Phys. **40**, 286 (2014).

[14] S. Moser, J. Electron Spectrosc. Relat. Phenom. **214**, 29 (2017).

[15] E. L. Shirley, L. J. Terminello, A. Santoni, and F. J. Himpsel, Phys. Rev. B **51**, 13614 (1995).

[16] A. Bostwick, T. Ohta, T. Seyller, K. Horn, and E. Rotenberg, Nat. Phys. **3**, 36 (2006).

[17] A. Bostwick, T. Ohta, J. L. McChesney, K. V. Emtsev, T. Seyller, K. Horn, and E. Rotenberg, New J. Phys. **9**, 385 (2007).

[18] M. Mucha-Kruczyński, O. Tsyplyatyev, A. Grishin, E. McCann, V. I. Fal'ko, A. Bostwick, and E. Rotenberg, Phys. Rev. B **77**, 195403 (2008).

[19] I. Gierz, T. Suzuki, R. T. Weitz, D. S. Lee, B. Krauss, C. Riedl, U. Starke, H. Höchst, J. H. Smet, C. R. Ast, and K. Kern, Phys. Rev. B **81**, 235408 (2010).

[20] W. S. Jung, C. S. Leem, C. Kim, S. R. Park, S. Y. Park, B. J. Kim, E. Rotenberg, and C. Kim, Phys. Rev. B **82**, 235105 (2010).

[21] P. Puschnig and D. Lüftner, J. Electron Spectrosc. Relat. Phenom. **200**, 193 (2015).

[22] C.-C. Lee, M. Fukuda, Y.-T. Lee, and T. Ozaki, arXiv:1707.02525.

[23] As shown in Ref. [72] it is actually possible to observe the full Fermi surface of graphene in ARPES by using s-polarized incident light. This phenomenon can be explained theoretically if scattering of the photoemitted state by the graphene lattice is taken into account. Such effects will not be considered in the present work.

[24] J. Voit, L. Perfetti, F. Zwick, H. Berger, G. Margaritondo, G. Grüner, H. Höchst, and M. Grioni, Science **290**, 501 (2000).

[25] P. Chen, Y. H. Chan, X. Y. Fang, Y. Zhang, M. Y. Chou, S. K. Mo, Z. Hussain, A. V. Fedorov, and T. C. Chiang, Nat. Commun. **6**, 8943 (2015).

[26] S. Chakravarty, C. Nayak, and S. Tewari, Phys. Rev. B **68**, 100504 (2003).

[27] A. Pal and E. J. Mele, Phys. Rev. B **87**, 205444 (2013).

[28] M. Mucha-Kruczyński, J. R. Wallbank, and V. I. Fal'ko, Phys. Rev. B **93**, 085409 (2016).

[29] R. Bistritzer and A. H. MacDonald, Phys. Rev. B **81**, 245412 (2010).

[30] M. Koshino, New J. Phys. **17**, 015014 (2015).

[31] C. Caroli, D. Lederer-Rozenblatt, B. Roulet, and D. Saint-James, Phys. Rev. B **8**, 4552 (1973).

[32] P. J. Feibelman and D. E. Eastman, Phys. Rev. B **10**, 4932 (1974).

[33] Notice that this is only true formally for the incommensurate case, not being true for any finite truncation of the matrix $\boldsymbol{H}_{\mathbf{k}}(\{\mathbf{G}_b\},\{\mathbf{G}_t\})$.

[34] C. Ortix, L. Yang, and J. van den Brink, Phys. Rev. B **86**, 081405 (2012).

[35] M. Yankowitz, J. Xue, D. Cormode, J. D. Sanchez-Yamagishi, K. Watanabe, T. Taniguchi, P. Jarillo-Herrero, P. Jacquod, and B. J. LeRoy, Nat. Phys. **8**, 382 (2012).

[36] J. R. Wallbank, A. A. Patel, M. Mucha-Kruczyński, A. K. Geim, and V. I. Fal'ko, Phys. Rev. B **87**, 245408 (2013).

[37] P. San-Jose, A. Gutiérrez-Rubio, M. Sturla, and F. Guinea, Phys. Rev. B **90**, 115152 (2014).

[38] G. J. Slotman, M. M. van Wijk, P.-L. Zhao, A. Fasolino, M. I. Katsnelson, and S. Yuan, Phys. Rev. Lett. **115**, 186801 (2015).

[39] J. Jung, A. M. DaSilva, A. H. MacDonald, and S. Adam, Nat. Commun. **6**, 6308 (2015).

[40] J. Jung, E. Laksono, A. M. DaSilva, A. H. MacDonald, M. Mucha-Kruczyński, and S. Adam, Phys. Rev. B **96**, 085442 (2017).
[41] I. Adawi, Phys. Rev. **134**, A788 (1964).
[42] G. D. Mahan, Phys. Rev. B **2**, 4334 (1970).
[43] W. Schaich and N. Ashcroft, Solid State Commun. **8**, 1959 (1970).
[44] W. L. Schaich and N. W. Ashcroft, Phys. Rev. B **3**, 2452 (1971).
[45] J. Pendry, Surf. Sci. **57**, 679 (1976).
[46] M. Lüders, A. Ernst, W. M. Temmerman, Z. Szotek, and P. J. Durham, J. Phys.: Condens. Matter **13**, 8587 (2001).
[47] This approximation is sometimes insufficient to explain the observed data as shown in Ref. [72]. In this case, multiple scatterings of the photoemitted electron by the lattice become important and a full solution of the Lippmann-Schwinger equation (28) is required.
[48] F. W. J. Olver, D. W. Lozier, R. F. Boisvert, and C. W. Clark, editors, *NIST Handbook of Mathematical Functions* (Cambridge University Press, New York, 2010).
[49] B. H. Bransden and C. J. Joachain, *Physics of Atoms and Molecules* (Longman Scientific & Technical, 1982).
[50] D. Belkić and H. S. Taylor, Phys. Scr. **39**, 226 (1989).
[51] N. Yükçü, AIP Conf. Proc. **1722**, 060009 (2016).
[52] F. Flicker and J. van Wezel, Phys. Rev. B **94**, 235135 (2016).
[53] P. San-Jose, A. Gutiérrez-Rubio, M. Sturla, and F. Guinea, Phys. Rev. B **90**, 075428 (2014).
[54] B. Amorim, A. Cortijo, F. de Juan, A. Grushin, F. Guinea, A. Gutiérrez-Rubio, H. Ochoa, V. Parente, R. Roldán, P. San-Jose, J. Schiefele, M. Sturla, and M. Vozmediano, Phys. Rep. **617**, 1 (2016).
[55] A. H. Castro Neto, F. Guinea, N. M. R. Peres, K. S. Novoselov, and A. K. Geim, Rev. Mod. Phys. **81**, 109 (2009).
[56] J. C. Slater and G. F. Koster, Phys. Rev. **94**, 1498 (1954).
[57] P. Moon and M. Koshino, Phys. Rev. B **87**, 205404 (2013).
[58] J. M. B. Lopes dos Santos, N. M. R. Peres, and A. H. Castro Neto, Phys. Rev. Lett. **99**, 256802 (2007).
[59] R. Bistritzer and A. H. MacDonald, Proc. Natl. Acad. Sci. USA **108**, 12233 (2011).
[60] J. M. B. Lopes dos Santos, N. M. R. Peres, and A. H. Castro Neto, Phys. Rev. B **86**, 155449 (2012).
[61] T. Ohta, J. T. Robinson, P. J. Feibelman, A. Bostwick, E. Rotenberg, and T. E. Beechem, Phys. Rev. Lett. **109**, 186807 (2012).
[62] The exchange of sublattices is due to the fact that the path $\Gamma_m \rightarrow \mathrm{M}_m \rightarrow \Gamma_m$ for the top layer is equivalent to the path obtained by exchanging $y \rightarrow -y$ for the bottom layer. With the chosen sublattice basis, the operation $y \rightarrow -y$ leads to the change $A \leftrightarrow B$.
[63] E. Cappelluti, R. Roldán, J. A. Silva-Guillén, P. Ordejón, and F. Guinea, Phys. Rev. B **88**, 075409 (2013).
[64] R. Roldán, M. P. López-Sancho, F. Guinea, E. Cappelluti, J. A. Silva-Guillén, and P. Ordejón, 2D Mater. **1**, 034003 (2014).
[65] W. A. Harrison, *Elementary Electronic Structure* (World Scientific, Singapore, 1999).
[66] A. Castellanos-Gomez, R. Roldán, E. Cappelluti, M. Buscema, F. Guinea, H. S. J. van der Zant, and G. A. Steele, Nano Lett. **13**, 5361 (2013).
[67] P.-C. Yeh, W. Jin, N. Zaki, J. Kunstmann, D. Chenet, G. Arefe, J. T. Sadowski, J. I. Dadap, P. Sutter, J. Hone, and R. M. Osgood, Nano Lett. **16**, 953 (2016).
[68] S. Huang, X. Ling, L. Liang, J. Kong, H. Terrones, V. Meunier, and M. S. Dresselhaus, Nano Lett. **14**, 5500 (2014).
[69] K. Liu, L. Zhang, T. Cao, C. Jin, D. Qiu, Q. Zhou, A. Zettl, P. Yang, S. G. Louie, and F. Wang, Nat. Commun. **5**, 4966 (2014).
[70] H. Haug and A.-P. Jauho, *Quantum Kinetics in Transport and Optics of Semiconductors*, 2nd ed., Springer Series in Solid-State Sciences, Vol. 123 (Springer-Verlag, Berlin, 2008).
[71] J. Rammer, *Quantum Field Theory of Non-equilibrium States* (Cambridge University Press, Cambridge, 2007).
[72] I. Gierz, J. Henk, H. Höchst, C. R. Ast, and K. Kern, Phys. Rev. B **83**, 121408 (2011).